HHS Public Access

Author manuscript

Nature. Author manuscript; available in PMC 2020 July 15.

Published in final edited form as:

Nature. 2020 January ; 577(7792): 689–694. doi:10.1038/s41586-019-1912-x.

VEGF-C-driven lymphatic drainage enables brain tumor immunosurveillance

Eric Song[1], **Tianyang Mao**[1], **Huiping Dong**[1], **Ligia Simoes Braga Boisserand**[2], **Salli Antila**[5], **Marcus Bosenberg**[1,3,4], **Kari Alitalo**[5], **Jean-Leon Thomas**[2,6,8,*], **Akiko Iwasaki**[1,3,7,8,*]

[1]Department of Immunobiology, Yale University School of Medicine, New Haven, CT, 06520, USA [2]Department of Neurology, Yale University School of Medicine, New Haven, CT, 06520, USA [3]Department of Dermatology, Yale University School of Medicine, New Haven, CT, 06520, USA [4]Department of Pathology, Yale University School of Medicine, New Haven, CT, 06520, USA [5]Translational Cancer Medicine Program and Wihuri Research Institute, Biomedicum Helsinki, University of Helsinki, FIN-00014, Helsinki, Finland [6]Institut du Cerveau et de la Moelle Épinière, INSERM U1127, CNRS UMR 7225, GH Pitié-Salpêtrière, Sorbonne Université, 75013 Paris, France [7]Howard Hughes Medical Institute, Chevy Chase, MD, 20815, USA [8]These authors jointly supervised this work: Jean-Leon Thomas, Akiko Iwasaki

Abstract

Immune surveillance against pathogens and tumors in the central nervous system (CNS) is thought to be limited due to the lack of lymphatic drainage. However, recent characterization of the meningeal lymphatic network sheds new light on previously unappreciated ways of eliciting immune response to antigens expressed in the brain[1–3]. Despite the remarkable progress made in our understanding of the development and structure of meningeal lymphatics, its contribution in evoking a protective antigen-specific immune response in the brain still remains unclear. Here we examine whether meningeal lymphatic vasculature can be manipulated to mount better immune responses against brain tumors. Using a mouse model of glioblastoma multiforme (GBM), we show that very limited CD8 T cell immunity to GBM antigen is elicited when the tumor is confined to the CNS, resulting in uncontrolled tumor growth. However, ectopic VEGF-C expression promotes enhanced CD8 T cell priming in the draining deep cervical lymph nodes, migration of CD8 T cells into the tumor and rapid clearance of the GBM, resulting in long-lasting antitumor memory response. Further, VEGF-C mRNA works synergistically with checkpoint

* jean-leon.thomas@yale.edu, akiko.iwasaki@yale.edu.

Author Contributions

E.S. J.L.T., and A.I. planned the project. E.S. and A.I. designed, analyzed and interpreted data and wrote the manuscript. E.S., L.B. and T.M. performed experiments and analyzed data. H.D. bred and cared for animals. J.L.T. provided AAV material. S.A., M.B. and K.A. provided expertise, materials and analysis of data.

Competing Interests

Akiko Iwasaki, Eric Song, and Jean-Leon Thomas have filed a patent related to the manuscript as inventors. Application number, US 62/768,390; status of application, provisional; specific aspect of manuscript covered in patent application. Kari Alitalo is an inventor of several patents related to VEGF-C. He or his wife currently have no income, stock or other benefits from companies related to work in the manuscript. Helsinki University is a shareholder in companies related to the use of VEGF-C. Marcus Bosenberg is a consultant for Eli Lilly and Company.

blockade therapy to eradicate existing GBM. These results reveal the capacity of VEGF-C to promote tumor immune surveillance, and offer a new therapeutic approach to treat brain tumors.

We utilized GL261, a C57BL/6 syngeneic cell line to model GBM. Orthotopic luciferase expressing GL261 (GL261-Luc) displayed cell number-dependent growth kinetics and lethality (Extended Data Fig 1a–c), demonstrating that intracranial injection of GL261-Luc is not sufficient to promote rejection in the CNS. To evaluate the effects of enhanced lymphangiogenesis, we delivered an established lymphangiogenesis-promoting factor, Vascular Endothelial Growth Factor C (VEGF-C), using AAV_9 (ref. [4]) and mRNA delivery vectors. Consistent with previous reports[1,4,5], injection of AAV-VEGF-C into cerebrospinal fluid (CSF) through the cisterna magna remodeled meningeal lymphatic vessels in the dural confluence of sinuses (Fig 1a–b) and sagittal sinuses (Extended Data Fig 1h–i) while showing no compromise in BBB integrity (Extended Data Fig 1d–e)[4]. In mice prophylactically treated with AAV-VEGF-C, we observed near-complete rejection of tumors (Fig 1c, Extended Data Fig 1j).

Previous studies show that deep cervical lymph nodes (dcLNs) are the primary draining lymph node of the CNS, with mandibular and superficial cervical lymph nodes contributing to CNS antigen sampling[1,3,6,7]. Thus, we surgically ligated the afferent lymphatic vessels draining to both dcLNs in AAV-VEGF-C-treated mice. Albeit having prolonged survival compared to control mice (Fig 1d), majority of AAV-VEGF-C treated mice succumbed to the tumor if their dcLNs were ligated; indicating that VEGF-C-mediated protection against GBM required lymph drainage to the dcLNs.

The requirement for the dcLNs suggested the role of the immune system in VEGF-C-mediated protection. Depletion of CD4 or CD8 T cells negated the protection conferred by VEGF-C (Fig 1e and Extended Data Fig 1k). In contrast, B cell-deficient μMT mice treated with VEGF-C were protected from GBM (Extended Data Fig 1l). We examined the durability of this immune response against GBM in VEGF-C-treated mice, and found mice that rejected the intracranial tumor showed long term systemic memory responses, as re-challenge with GL261-Luc in the flank resulted in no detectable tumor (Fig 1f and Extended Data Fig 1m). Together, these data demonstrate that by increasing lymphangiogenesis in the meninges, prophylactic VEGF-C treatment can evoke a robust and long-lasting T cell-dependent immune response against brain neoplasms.

Others have observed tumor-intrinsic VEGF-C overexpression in mouse or human results in poorer prognosis in malignancies outside the CNS[8,9]. We compared transcriptomes of healthy brain tissue versus GBM tissue from patients using data from GTEX and TCGA, respectively. Tumor tissue showed higher levels of VEGF-A and CD31, as previously shown[10], but a decrease in VEGF-C (Fig 2a–c, Extended Data Fig 2a–b), which was also seen in GBM-bearing mice (Extended Data Fig 2c). Stratifying patients into high vs. low VEGF-C groups showed no survival differences (Extended Data Fig 2d–e), as even the high VEGF-C group had lower expression levels than healthy brain. However, a recently published dataset of GBM patients treated with neoadjuvant anti-PD-1 (Ref. [11]) showed high correlation of VEGF-C with increased T cell infiltration (CD3e, CD4, CD8B) after treatment (Fig 2d–f). Collectively, these results suggest that, 1) GBM microenvironment is deprived of

lymphangiogenic signals in both patients and in experimental animals, and 2) ectopic VEGF-C confers protection against GBM in a mouse model.

Although AAV-VEGF-C showed survival benefits with no long-term side effects (Extended Data Fig 1d–e and g), AAV is less effective when given subsequently to the same host due to its immunogenicity[12], in contrast to mRNA delivery[13]. Therefore, we designed mRNA coding for VEGF-C (VEGF-C-mRNA) with stabilizing base substitutions (Extended Data Fig 3a–b); transfection of HEK293T cells with this construct produced both full-length and processed VEGF-C forms[14] (Extended Data Fig 3c). Administration of VEGF-C-mRNA into the cisterna magna resulted in high levels of VEGF-C in the CSF (Extended Data Fig 3d). We utilized Cy5 labeled mRNA to confirm wide distribution of the mRNA within the dura mater (Extended Data Fig 3f) and saw uptake by cells in the brain, meninges and the dcLNs, amongst immune (CD45+), endothelial (CD45-CD31+) and other cells (CD45-CD31-) (Extended Data Fig 3g–h). Further, we observed increased secreted VEGF-C protein specific to the CSF and meninges, with no changes in the brain or serum (Extended Data Fig 3i). Using AKT phosphorylation to measure VEGFR signaling in endothelial cells after VEGF-C treatment, we observed specific signaling increases within the lymphatic endothelial cell (LEC) population, with no changes in the blood endothelial cells (BEC) in the meninges or dcLNs (Extended Data Fig 4a–c). This increase was not accompanied by structural deformities in either the LECs or BECs even within an angiogenic tumor environment (Extended Data Fig 4b–d). These data indicated that while VEGF-C-mRNA was taken up by various cells of the brain, meninges and dcLN, VEGF-C protein was mostly confined to the CSF and meninges, activating LECs.

In addition to the difference in immunogenicity, expression kinetics of VEGF-C-mRNA and AAV-VEGF-C diverge, with the former showing peak expression after 24 h and the latter showing maximal expression after several weeks[15]. We evaluated the therapeutic efficacy of both modalities by administrating each on different days, and saw that only prophylactic (-d60) AAV-VEGF-C resulted in long-term survivors (Extended Data Fig 4f–h). In contrast, using VEGF-C-mRNA monotherapy administered at days 0, 3 or 7, survival benefits were still observed, although none of these treated-mice survived in the face of rapid GBM development (Extended Data Fig 4f).

Similarly, anti-PD-1 and other checkpoint blockade therapies show little benefit against GBM as a monotherapy in preclinical models[16,17], and have not shown beneficial responses in clinical trials[18]. However, strategies that promote T cell responses, such as activation of dendritic cells[19], or radiation[16] potentiate anti-PD-1 therapy against GBM, suggesting that hurdles in CNS cancer treatment may be during T cell priming. Hypothesizing that VEGF-C increases immune surveillance of the brain, we reasoned that such a therapy would have synergistic anti-tumor effects with checkpoint inhibitor therapy. While anti-PD-1 alone had marginal effects on survival, the combination of VEGF-C-mRNA with anti-PD-1 antibody resulted in regression of tumors and survival benefits in mice bearing established GL261 tumors (Fig 3b) in a T cell dependent manner (Extended Data Fig 5d). The long-term surviving mice re-challenged with tumors in the contralateral hemisphere showed resistance to the secondary challenge (Extended Data Fig 5b), and T cells transferred from the draining lymph nodes and spleen of mice that rejected tumors conferred protection against a primary

challenge (Extended Data Fig 5c). A survival benefit was also observed in mice bearing a more proliferative and invasive syngeneic GBM cell line, CT2A, after a combination of VEGF-C-mRNA and anti-PD-1 plus anti-41BB[20] administration (Extended Data Fig 5e–g). In addition, other checkpoint inhibitors that are known to be ineffective[16,17,21] were potentiated with VEGF-C-mRNA (Extended Data Fig 5h–j). Even when mice were treated after significant amount of the tumor mass (day 20), the combination therapy showed survival benefits (Extended Data Fig 5k and l).

To assess if T cell priming against GBM in the dcLN was increased after VEGF-C treatment, we used an endogenous tumor antigen present in many mouse cancers[22]. Endogenous retroviruses (ERVs) are integrated retrovirus remnants in the host genome that are silenced epigenetically, but often become aberrantly expressed in dysregulated transcriptional states found in cancers[23]. We identified *emv2*-based ERV sequences overexpressed in GL261 (Extended Data Fig 6a–b). Tetramers against emv2-env[22], showed an enrichment of tetramer positive CD8 T cells in the draining inguinal lymph nodes after administration of GL261 in the flank of mice (Extended Data Fig 6d), demonstrating endogenous tumor specific antigen-dependent T cell priming in response to GL261.

Intracranial GL261-Luc inoculation resulted in small tetramer positive T cell populations in dcLNs (1.54%) (Fig. 3c–d). However, VEGF-C-mRNA allowed for significant increases in the tumor-specific T cell population in the dcLN (3.65%) (Fig. 3c–d). In addition, increase in both percent (Fig 3d) and absolute numbers (Extended Data Fig. 5a) of tumor-specific T cell infiltration was detected in the brain after VEGF-C-mRNA treatment. These data reveal that intracranial tumor elicits minimal CD8 T cell responses in the dcLN. However, VEGF-C-mRNA enhanced CD8 T cell priming against tumors in the brain.

We then examined the specificity of VEGF-C potentiating checkpoint inhibitor therapy. First, to confirm the requirement of meningeal lymphatics, a soluble VEGFR-$3_{1–3}$-Ig (AAV-sVEGFR-3) was administered to sequester VEGF-C, resulting in atrophy of lymphatic vasculature in the dura[4,24] (Extended Data Fig 7a–b). VEGFR-$3_{1–3}$-Ig abrogated the efficacy of VEGF-C-mRNA and anti-PD-1 therapy (Extended Data Fig 7c). VEGF-C also uniquely provided therapeutic benefits in combination with anti-PD-1 compared to other recombinant VEGF family proteins (A, B, Cs and D; Cs being Cys156Ser, a VEGFR3 selective agonist) (Extended Data Fig 7d–f). These experiments establish the specificity of the antitumor capacity of VEGF-C, and the requirement for the meningeal lymphatics in providing therapeutic benefits against GBM.

Tumor-intrinsic VEGF-C also was reported to mediate increased metastases in melanoma and breast cancer[9,24,25]. To evaluate if this was a possibility in the CNS, tumor cells expressing blue fluorescence protein (BFP) were used to track their distribution *in vivo*. We collected the brain and dcLNs to measure tumor cells (CD45-BFP+), and immune cells that may have phagocytosed tumor cells (CD45+BFP+). VEGF-C treatment resulted in no CD45-BFP+ cells in the dcLNs, suggesting that VEGF-C does not promote lymph node metastasis of GBM (Extended Data Fig 7g–k). In addition, direct effects of VEGF-C on tumor cells are unlikely, as GBM cells showed no expression of VEGFR-3, and no impact on proliferation in culture with VEGF-C (Extended Data Fig 7l–m). Of note, both forms of

VEGF-C resulted in increased CD45+BFP+ cells in the dcLNs (Extended Data Fig 7i), consistent with reports that antigen drainage is increased by exogenous VEGF-C[1,2].

To examine how VEGF-C modifies the tumor immune landscape prior to anti-PD-1 therapy, we performed flow cytometry in the brain, meninges and dcLNs after VEGF-C-mRNA treatment. Myeloid population numbers showed minimal changes, with no differences in activation levels (CD80) or antigen presentation capabilities (MHCII) (Extended Data Fig 8a–g). The largest change induced was in the number and the phenotypes of T cells infiltrating the brain (Fig 3e and Extended Data Fig 9a). This result, combined with increased CD45+BFP+ cells in the dcLNs (Extended Data Fig 7i), suggested that the increased priming of T cells and subsequent infiltration of T cells resulted from increased antigen drainage. VEGF-C also showed sustained TCF7+ CD8 T cells, a population important for eliciting anti-tumor effector responses[26,27], (Extended Data Fig 9c–f) in the three compartments along with increased FOXP3+ CD4 T cells (Extended Data Fig 9f). Interestingly, higher proportion of FOXP3+ cells expressed T-bet, a critical regulator of the T helper 1 (Th1) differentiation (Extended Data Fig 9f), which is associated with increased IFNγ in Tregs and reduced suppression of CD4 effector cells[28]. These data indicate a shift towards an anti-tumor immune response in the VEGF-C treated mice. Consistent with this, CD8 T cells in the brain were also poised to produce multiple cytokines after *ex vivo* stimulation (Extended Data Fig 9e–i), a positive prognostic factor for immunotherapy[29]. All of these changes seemed to be independent of direct effect on T cells, as no VEGFR-3 expression was detectable (Extended Data Fig 7n), and VEGF-C did not affect T cell proliferation *in vitro* (Extended Data Fig 7p). We also did not observe VEGFR-3 expression in other immune compartments, and BMDC stimulation with VEGF-C induced no change in MHCII or costimulatory molecule expression levels (Extended Data Fig 7o). Altogether, these results highlight a potent anti-tumor environment provided by VEGF-C, associated with increased lymphatic drainage and antigen presentation to promote multifunctional and durable anti-GBM T cell immunity.

Unlike what is seen in GBM patients, recent reports showed that combined nivolumab and ipilimumab therapy had intracranial efficacy, concordant with extracranial activity, in patients with melanoma brain metastases[30]. In agreement with clinical observations, mice with both a flank (FT) and intracranial tumor (IC) responded better to immunotherapy compared to those just bearing an intracranial melanoma[31]. To examine whether VEGF-C-mRNA is effective in treating non-GBM cancer types in the CNS, we used melanoma cell lines, YUMMER1.7 and B16 (Extended Data Fig 10a). Mice bearing only YUMMER1.7 IC showed significant survival benefits when given VEGF-C-mRNA and checkpoint inhibitor therapy (Fig 4a). In contrast, mice with both IC and FT saw benefits from checkpoint inhibitor therapy regardless of VEGF-C-mRNA treatment (Fig 4b). In fact, mice with only IC receiving combination therapy had similar survival benefits as those with both IC and FT and treated with checkpoint inhibitor therapy (Fig 4c). Additionally, ligation of the dcLNs only affected mice with IC, and not mice with both IC and FT (Fig 4a–b). Similar results were observed with B16 (Extended Data Fig 10c–e). These results are consistent with the idea that T cell priming, either via CSF VEGF-C expression or a flank tumor, enables efficient checkpoint inhibitor responses in the CNS. However, in the case of a tumor

confined to the CNS at steady state, regardless of tumor type, immune checkpoint inhibitors alone do not exhibit significant benefits.

Finally, we sought to understand whether the anti-tumor effects of VEGF-C is due to the expansion and differentiation of T cells capable of trafficking to the brain (T cell intrinsic), or to changes in the brain environment increasing T cell recruitment (T cell extrinsic). We performed adoptive transfer of leukocytes from the draining lymph node of tumor bearing mice into the recipient mice also bearing tumors (Fig 4d–e). T cell infiltration into the brain was slightly increased (T cell intrinsic = 1.6-fold increase) if the T cells were from VEGF-C-mRNA treated mice. However, T cells from tumor-bearing control mice were able to migrate into the brain with GBM, to a greater extent, if recipient was treated with VEGF-C-mRNA (T cell extrinsic = 3.1-fold increase) (Fig 4e). Moreover, donor T cells from VEGF-C treated animal transferred into VEGF-C treated host were able to most efficiently infiltrate the tumor (Combinatorial = 4.2-fold increase). Increases in T cell numbers in the lymph node was dependent on the recipient mice having VEGF-C-mRNA treatment, in agreement with the idea that antigen specific T cells proliferate only after increased drainage of tumor antigen from the CNS. These results show that VEGF-C provides an anti-tumor environment through a combination of its effect on the meningeal lymphatic vasculature and changes in T cell intrinsic properties.

We have demonstrated the potential to manipulate meningeal lymphatics with ectopic VEGF-C to confer immune surveillance and T cell mediated immunity against brain tumors (Extended Data Fig 10g). These results support the growing knowledge on the importance of meningeal lymphatics in controlling CNS immune responses[3–5]. The lack of immune responses against tissue grafts[32] in the CNS led to the idea of immuneprivileged nature of the brain, and a similar phenomenon is perhaps what also allows for primary brain tumors like GBM to grow in the CNS unhindered[33]. Collectively, these reports, combined with our study, suggest that tumors confined within the CNS may be inaccessible for immune priming, and that exogenous VEGF-C potentiates endogenous immune responses. We considered the possibility of immune or tumor cell-intrinsic VEGF-C signaling causing this phenomenon, but found no changes in immune or tumor cells after direct VEGF-C stimulation. Instead, our data suggest that VEGF-C and its relationship with its main receptor partner, VEGFR-3, results in increased lymphatic drainage[34] necessary for immunosurveillance against GBM, similar to melanoma-intrinsic VEGF-C overexpression enhancing anti-tumor T cell responses[8]. It is worth noting that, the immuneprivileged status of the CNS does not apply to all brain antigens[6] and future studies are needed to define the rules of CNS antigen sampling. Altogether, our study shows that increasing lymphatic drainage can overcome the immune ignorance of GBM, and lays foundation for a new strategy of modulating lymphatic vasculature to increase effects of checkpoint inhibitor therapy against tumors in immune privileged sites.

Methods

Mice

Four- to eight-week-old mixed sex C57BL/6 mice, B6.129S2-*IghtmICgn*/J (μMT) mice, B6.SJL-Ptprc^{a}Pepc^{b}/BoyCrl mice, were purchased from the National Cancer Institute,

Jackson Laboratory and Charles River respectively and subsequently bred and housed at Yale University. All procedures used in this study (sex-matched, age-matched) complied with federal guidelines and institutional policies by the Yale School of Medicine Animal Care and Use Committee.

Cells

GL261 parental cells were obtained from the NIH cancer cell repository. GL261-Luciferase cells were kind gifts from Dr. Jiangbing Zhou (Yale Neurosurgery) and Dr. Carla Rothlin (Yale Immunobiology). YUMMER 1.7 cell lines are previously reported[35]. CT2A and CT2A-BFP cells were a kind gift from Dr. Thomas Mathivet (PARCC, Paris). B16 cells were a kind gift from Dr. Noah Palm (Yale Immunobiology). HEK293T cells were purchased from ATCC. HEK293T, CT2A, CT2A-BFP and B16 cells were cultured in complete DMEM (4.5g/L glucose, 10% FBS, 1% penicillin/streptomycin). YUMMER 1.7 cells were cultured in DMEM/F12 media (10% FBS, 1% nonessential amino acids, 1% penicillin/streptomycin). GL261 and GL261-Luc cells were cultured in RPMI (10% FBS, 1% penicillin/streptomycin).

Viral vectors

We used AAV_9 encoding either human VEGF-C, mouse VEGF-C or soluble mVEGFR3. AAV_9-mouse VEGF-C was generated using psubCMV WPRE plasmid as previously reported for human VEGF-C[4]. Control AAV_9–mouse Vegfr34–7-Ig encodes the domains 4–7 of mouse Vegfr3 (that do not bind VEGF-C or VEGF-D) fused to the mouse IgG1 Fc domain. mVEGFR3(1–3)-Ig, encoding the domains 1–3 of mouse Vegfr3, was used to sequester VEGF-C *in vivo*. Young mice (2–4 week-old, AAV-mVEGFR-3; 4–6 week-old, AAV-VEGF-C) received i.c.m injection of a single AAV dose (3×10^{12} viral particles/mouse/3μl) of AAVs. After 6–8 weeks, they were engrafted with intra-cerebral GL261 or CT-2A GBM cells.

Antibodies and tetramer

Anti-CD45 (30-F11, APC-Cy7, B266564; 104, BUV737, 9051755; 104, PE-Cy7, B268066; A20, APC, B254042; 30-F11, BV605, B278000), anti-CD3 (17A2, BV605, B264993; 145–2C11, APC-Cy7; 17A2, BUV737, 9042537; 17A2, Biotin, B259691), anti-CD4 (GK1.5, Pacific Blue, B199050; GK1.5, BUV496, 8080653), anti-CD8 (53–6.7, BV711, B259953; 53–6.7, BUV395, 8306672), anti-IFNγ (XMG1.2, BV711, B236526), anti-GZMB (GB11, FITC, B275568), anti-TNFα (MP6-XT22, PE-Cy7, B251190), anti-IL2 (JES6–5H4, APC, B248053), anti-CD44 (IM7, A700, B244378), anti-TBET (4B10, BV711, B268785), anti-TIM3 (RMT3–23, BV605, B262042), anti-FOXP3 (FJK-16s, BV421, B266620), anti-TCF7 (C63D9, A488, 8, Cell Signaling Technology), anti-PD-1 (29F.1A12, APC-Cy7, B260172), anti-RORγT (B2D, APC, E16663–102), anti-CD40 (PE, E028955), anti-CD80 (16–10A1, BUV395; 16–10A1, FITC, E029730), anti-CD86 (APC, B175381), anti-CX3CR1(SA011F11, BV421, B231871), anti-Ly6C (AL21, FITC, 33380), anti-CD11c (N418, PE-Cy7, B264758; BV421, B264454), anti-CD11b (M1/70, PE, B228654), anti-Ly6G (IA8, APC-Cy7, B153128), anti-MHCII (M5/114.15.2, A700, B264454), anti-CD64 (X54–5/7.1, APC, B254424), anti-B220 (RA3–6B2, BUV496, 8096734), anti-NK1.1 (PK136, biotin, B255213), anti-CD19 (6D5, biotin, B250292), anti-F4/80 (BM8, biotin,

B253458), anti-Podoplanin (eBio8.1.1, PE, E11344–399, eBioscience), anti-CD31 (390, A647, 8187629), anti-AKT (pS473) (M89–61, BV421, 7198801) antibodies were purchased from BioLegend (Bxxxxxx) or BD Biosciences (xxxxxxx). anti-VEGFR-3/FLT-4 (FAB743P, PE, ACBF0117091) antibodies were purchased from R&D biosciences. K^b-restricted peptides aa 604–611 of p15E protein (KSPWFTTL) tetramer was made through the NIH tetramer core facility. KSPWFTTL peptide was made by Biomatik Corporation (Ontario, CA). Depletion antibodies anti-CD4 (GK1.5), anti-CD8 (YTS169.4), anti-PD1 (RMP1–14), anti-CTLA4 (9H10), anti-TIM3 (RMT3–23), anti-4–1BB (LOB12.3) antibodies were purchased from BioXCell (West Lebanon, NH).

VEGF-C-mRNA

VEGF-C-mRNA (Extended Data Fig 2) was made by TriLink BioTechnologies (San Diego, CA), with full substitution of pseudo-uridine and 5-methyl-cytosine bases, capped using CleanCap™ AG and polyadenylated (120A). mRNA was mixed at a ratio of 1μg / 0.1μL of *in vivo*-jetPEI (Polyplus transfection, France) and vortexed for 30 seconds and incubated in room temperature for 15 minutes before use. Control mRNA (Cy5 labeled GFP, GFP-mRNA; Luciferase, Luc-mRNA) was also purchased from TriLink Biotechnologies. Recombinant proteins (VEGF-A, VEGF-B, VEGF-C Cys156Ser, VEGF-D) were purchased from R&D systems.

Tissue processing and microscopy

Meningeal lymphatic vessels were detected on whole-mount preparation of the dura matter. Skullcap samples were dissected, fixed in 2% PFA for one hour and promptly processed in a blocking solution (10% normal donkey serum, 1% bovine serum albumin and 0,3% PBS-Triton X-100) for overnight incubation at 4°C. For lymphatic vessel detection, samples were incubated with the primary antibody anti-LYVE-1 (AngioBio, #11–034, 1:400), overnight at 4°C, then washed in PBS and 0.5% Triton X −100, five times at room temperature, before incubation with a fluoro-conjugated secondary antibody (Alexa Fluor anti-rabbit 647 Thermo Fischer, 1:500) diluted in PBS and 5% normal donkey serum. Meningeal lymphatic vessel images were acquired using a spinning-disk confocal (Nikon Eclipse T*i*). Quantitative analysis of meningeal lymphatic coverage was performed using either FIJI or ImageJ (NIH/Bethesda) image processing software. LYVE-1^+ macrophages that are less intensely labeled than lymphatic vessels were eliminated by adjusting image contrast. Otsu's threshold was then used to convert captured images into binary images. The fluorescence labeled area covered by meningeal lymphatic vessels was measured in the confluence of sinuses and the sagittal sinus regions, and was normalized to the average fluorescence of the same regions of meningeal lymphatic vasculature in CTRL-AAV-treated mice. For brain sections, anti-CD3 (17A2, biotin), anti-CD31 (2H8, GeneTex) and anti-LYVE1 (AF2125, R&D systems) antibodies were used with anti-streptavidin (FITC, BD biosciences, 4031801), anti-hamster (127–165-160, Cy3, Jackson ImmunoResearch, 128827), and anti-goat (705–175-147, Cy5, Jackson ImmunoResearch, 138513) secondary antibodies respectively. Confocal images were taken on a Leica SP8. 3D rendering was completed on Imaris 8 (Oxford Instruments).

Western blot

HEK293T cells were transfected with VEGF-C-mRNA combined with lipofectamine. Samples were lysed in RIPA buffer and boiled for 5 minutes with sample buffer. For in vivo delivery, VEGF-C-mRNA with JETPEI was used. CSF was pooled from 10 animals and spun down to remove cells. CSF was then filtered using a 100k Amicon filter and the wash through was boiled with sample buffer for western blot. Western blot was performed similarly to previously reported[2]. Briefly, 15% gels were used and run at 10 A per gel for 30 minutes and 40 A per gel until separation of ladder. Wet transfer was performed at 120 A per gel for 90 minutes on ice. Anti-VEGF-C antibody was used at a concentration of 1:1000 (R&D systems, AF752) and incubated overnight in the cold room. After washing, anti-Goat-HRP secondary antibodies were used at a concentration of 1:5000 at room temperature for 2 hours and imaged using ChemiDoc MP imaging system (Biorad).

Procedures

Tumor inoculation—Animals were anaesthetized using a mixture of ketamine (50 mg kg^{-1}) and xylazine (5 mg kg^{-1}), injected intraperitoneally. Mice heads were shaved and then placed in a stereotaxic frame. After sterilization of the scalp with alcohol and betadine, a midline scalp incision was made to expose the coronal and sagittal sutures, and a burr hole was drilled 2 mm lateral to the sagittal suture and 0.5 mm posterior to the bregma. A 10 μl Hamilton syringe loaded with tumor cells, was inserted into the burr hole at a depth of 2.5 mm from the surface of the brain and left to equilibrate for 1 min before infusion. A micro-infusion pump (World Precision Instruments, Sarasota, FL, USA) was used to infuse 3 μl of tumor cells at 1 μl min^{-1}. Once the infusion was finished, the syringe was left in place for another minute before removal of the syringe. Bone wax was used to fill the burr hole and skin was stapled and cleaned. Following intramuscular administration of analgesic (Meloxicam and buprenorphine, 1 mg kg^{-1}), animals were placed in a heated cage until full recovery.

Intra-Cisterna Magna (i.c.m), CSF collection—For i.c.m. injections, mice were anesthetized using ketamine and xylazine, and the dorsal neck was shaved and cleaned with alcohol. A 2 cm incision was made at the base of the skull, and the dorsal neck muscles were separated using forceps. After visualization of the cisterna magna, a Hamilton syringe with a 15 degree 33 gauge needle was used to puncture the dura. 3μL of AAV_9 (3.10^{12} viral particles/mouse) or mRNA (4–5 μg) was administered per mouse at a rate of 1μL min^{-1}. Upon completion of the injection, needle was left in to prevent backflow for an additional 3 minutes. For CSF collection, a custom pulled micro pipette 0.75/1 1brl GF (Stoelting co) was used to penetrate the dura and made sure no blood was collected. The skin was stapled, cleaned and same post-operative procedures as tumor inoculations were performed.

Deep cervical lymph node ligation—For lymph node ligation, mice were anesthetized using ketamine and xylazine, and the rostral neck was shaved and disinfected. A 2 cm incision was made and the salivary glands containing the superficial cervical lymph nodes were retracted and deep cervical lymph nodes were visualized. The afferent lymph nodes were tied off with a 4–0 Vicryl suture, and then cauterized. The incision was closed with 4–0 Vicryl suture and mice were subjected to the same post-operative procedures as above.

Flank tumor inoculation—Mice were anesthetized using ketamine and xylazine. Flank was shaved and disinfected. A 1mL syringe with 30g needle was used to deliver 100 μL of 500,000 cells subcutaneously. For GL261-Luc cells, cells were mixed in a 1:1 volume with Matrigel (Corning) before delivering.

Adoptive Transfer

To evaluate memory against tumor using adoptive transfer, T cells from deep cervical lymph nodes and spleens of mice that rejected tumors after VEGF-C-mRNA and α-PD-1 treatment were isolated using EasySep Mouse T cell Isolation Kit (StemCell Technologies, Canada) and transferred into naïve mice 24 h before tumor inoculation (one mouse T cells to one mouse).

To study leukocyte trafficking after VEGF-C treatment, CD45.2 mice were inoculated with GL261 tumors. At day 7, Mice were given GFP-mRNA or VEGF-C-mRNA treatment. At day 7 post-treatment, deep cervical lymph nodes were collected, filtered through 70μm filter paper and whole leukocyte suspensions (30 million cells per mouse; roughly ~3–5 mouse dCLNs transferred into one mouse) were adoptively transferred in to CD45.1 mice bearing 7 day old tumors. After transfer, mice were given GFP-mRNA or VEGF-C-mRNA treatment i.c.m. 5 days after, deep cervical lymph nodes and brain tissue were collected to evaluate immune cell trafficking. 5 minutes prior to euthanizing the mouse, 25μg of anti-CD45 PE (30-F11, PE, Biolegend) antibodies were administered intravenously to stain circulating immune cells.

IVIS imaging

Mice were anesthetized using isoflurane and injected intraperitoneally with RediJect D-Luciferin Ultra (PerkinElmer) (200μL, 30mg/mL). After 10 minutes mice were imaged using the IVIS Spectrum In Vivo Imaging System (PerkinElmer).

RNA-seq

RNA-seq data was aligned using STAR (STAR/2.5.3a-foss-2016b, mm10 assembly) with parameters: --runThreadN 20 --outSAMtype BAM SortedByCoordinate --limitBAMsortRAM 35129075129 --outFilterMultimapNmax 1 --outFilterMismatchNmax 999 --outFilterMismatchNoverLmax 0.02 --alignIntronMin 20 --alignIntronMax 1000000 --alignMatesGapMax 1000000 for mapping of repetitive elements. Counts were counted using BEDTools (BEDTools/2.27.1-foss-2016b), coverageBed function, normalized using DESEQ2 and graphed using broad institute Morpheus web tool. Human RNA-seq data was obtained from TCGA and GTEX databases and analyzed using the above parameters (hg38 assembly) (Extended Data Fig 2a–c), and survival stratified by VEGF-C expression was analyzed using OncoLnc (www.OncoLnc.org) (Extended Data Fig 2e–f).

Isolation of mononuclear cells and flow cytometry

Tissue was harvested and incubated in a digestion cocktail containing 1 mg ml−1 collagenase D (Roche), 1 mg ml−1 collagenase A (Roche) and 30 μg ml−1 DNase I (Sigma-Aldrich) in complete RPMI (10% FBS) at 37 °C for 30 min. Tissue was then filtered through a 70 μm filter. For brain tissues, cells were mixed in 4 mL of 25% Percoll (Sigma-Aldrich)

solution and centrifuged at 530g for 15 minutes without a brake. The Percoll layer was removed and cells were diluted in 5 mL of 1% BSA. Cells were treated with ACK buffer, and resuspended in 1% BSA. At this point cells were counted using an automated cell counter (Thermo fisher).

For tetramer experiments, staining was performed with antibodies (1:200) and tetramer (1:50) for 60 minutes at room temperature. Cells were washed to remove excess antibodies and resuspended in 1% BSA with 10 μL of CountBright absolute counting beads (Life technologies, OR) for multiparameter analyses on the LSR II flow cytometer (Becton Dickinson), and subsequently analyzed using FlowJo software (10.5.3, Tree Star). For calculation of tetramer positive T cells in each organ this calculation was used:number of tetramer positive T cells * (# of input beads / # of counted beads) * (# of cells from automated counter / # of total events in flow cytometry).

For cytokine stimulation, surface markers were first stained on ice for 30 minutes. After washing, cells were stimulated in complete RPMI with 200μL of 1x Cell stimulation cocktail without protein transporter inhibitor (eBioscience Cell Stimulation Cocktail, ThermoFisher) for 1 hour at 37C. 50 μL of 5x Cell stimulation cocktail with protein transporter (eBioscience Cell Stimulation Cocktail, ThermoFisher) was added and incubated for an additional 4 hours. Cells were then fixed with 100μL 2% formaldehyde on ice for 45 minutes. Cells were washed with 1x Perm/Wash Buffer (BD Cytofix/Cytoperm, BD Biosciences), and then permeabilized with 1x Perm/Wash Buffer (BD Cytofix/Cytoperm, BD Biosciences) for 10 minutes on ice. Intracellular antigens were stained on ice for 30 minutes.

For transcription factor staining, surface markers were first stained on ice for 30 minutes. Cells were then fixed with 100μL 2% formaldehyde on ice for 45 minutes. Cells were washed with 1x Perm/Wash Buffer (eBioscience Foxp3/Transcription Factor Staining Buffer Set, ThermoFisher), and then permeabilized with 1x FOXP3Perm/Wash Buffer for 10 minutes on ice. Intracellular antigens were stained on ice for 30 minutes.

For AKT phosphorylation staining, surface markers were first stained on ice for 30 minutes. Cells were then fixed and washed following BD Phosflow kit directions. Samples were run on Attune NxT Flow Cytometer.

ELISA

ELISA was performed using a Mouse Vascular Endothelial Cell Growth Factor C, VEGF-C ELISA Kit, by Cusabio LLC (lifeome, Oceanside CA, E07361m-96) following the manufacturer’s instructions.

mRNA Tropism

Mice were injected in the cisterna magna with Cy5 labeled GFP mRNA with JETPEI. 24 h post injection, brains, meninges and lymph nodes were collected for flow cytometry. Samples were run on Attune NxT Flow Cytometer.

BBB permeability

Mice were injected intravenously with 70,000 MW Fluorescein labeled Dextran (ThermoFisher) or 0.5% Evans Blue (EB). For microscopy, brains were collected 2 hours after and flash frozen for sectioning. For EB quantification, mice were perfused with ice cold PBS intraventricularly (heart) and EB was extracted using Dimethylformamide. Relative absorbance was measured using SpectraMax i3 (Molecular Devices) at 620nm wavelength.

T cell proliferation

T cells were isolated using EasySep Mouse T cell Isolation Kit (StemCell Technologies, Canada). T cells were stained using CellTrace Violet, and stimulated with CD3/CD28 antibodies from Bioxcell for 24 hours in cRPMI. After 24 h, cells were resuspended in media containing IL-2 and VEGF-C for 4 days and FACS was performed at the end of 4 days.

BMDC culture and Stimulation

Bone marrow was collected from wild type mice and cultured in cRPMI supplemented with GM-CSF for six days. After six days, cells were stimulated with LPS and VEGF-C for 24 h and FACS was performed.

Statistical analysis

No statistical methods were used to predetermine sample size. The animals getting treatment were randomized after tumor size measurement at day seven. The investigators were not blinded during experiments and outcome assessment, but outcome assessment was additionally evaluated by animal technicians and vets blinded to the study.

Survival curves were analyzed using a log-rank (Mantle-Cox) test. For other data, normally distributed continuous variable comparisons used a two-tailed unpaired Student's *t*-test or paired Student's *t*-test with Prism software.

Graphical Illustrations

Graphical illustrations were made with Biorender.com

Data availability

No new sequencing data were generated for this study. All datasets generated and/or analyzed during the current study are available in the article, the accompanying Source Data or Supplementary Information.

Code availability

All code used for analysis are in the methods and detailed files will be made available from the corresponding author upon request.

Extended Data

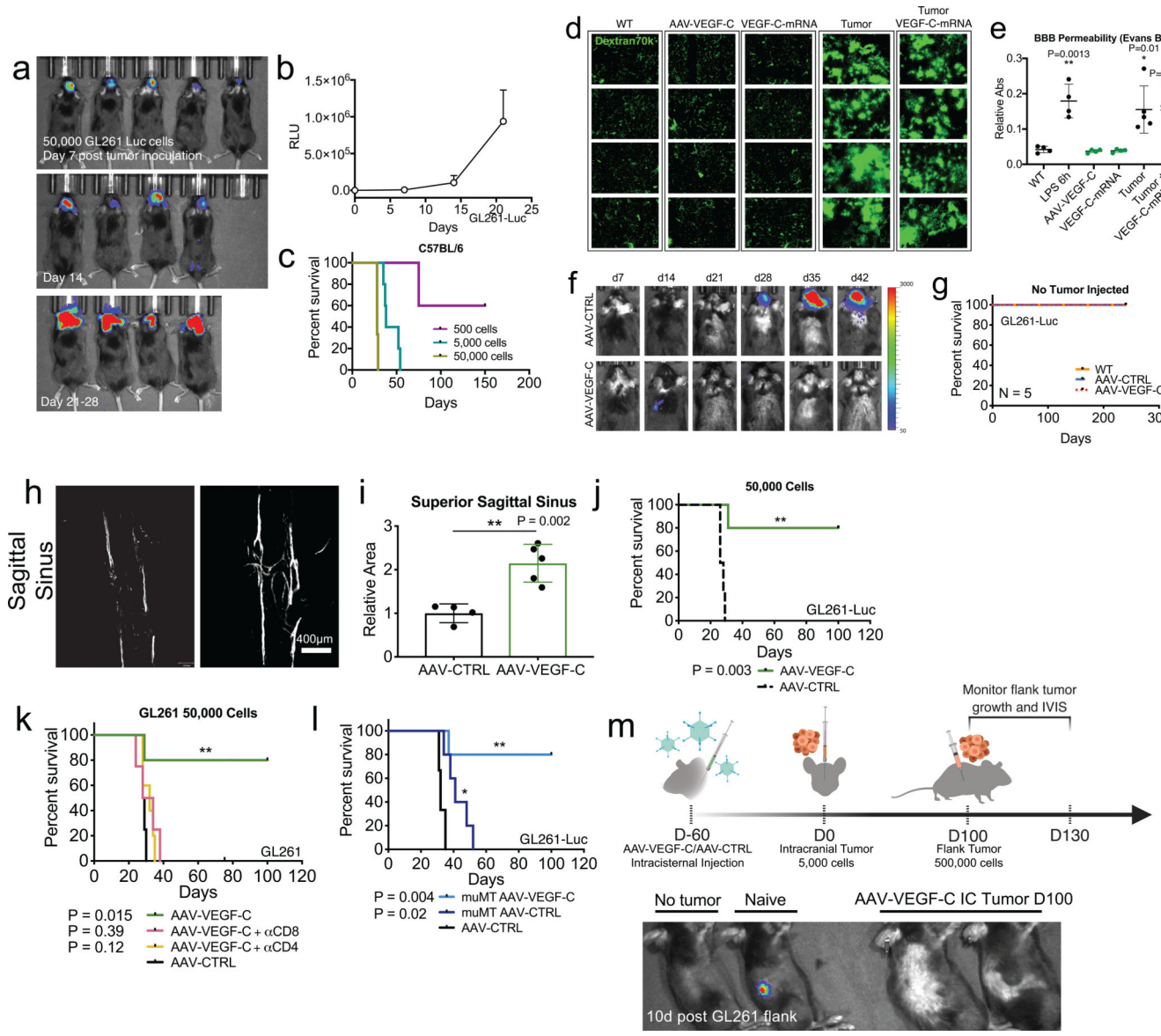

Extended Data Fig 1. Increased meningeal lymphatic vasculature confers protection against intracranial glioblastoma challenge in a draining lymph node and T cell dependent manner and provides long-term protection without BBB perturbance.

a-b Mice inoculated with 50,000 GL261-Luc cells were imaged every 7 days and showed consistent and reliable tumor growth (n = 4). **c** GL261-Luc shows lethality in mice in a cell number dependent way (500 cells, n = 5; 5000 cells, n = 5; 50,000 cells, n = 9). **d** Mice were injected I.V. with 70k MW Dextran-fluorescein and euthanized after 2 hours. Brains were collected and cryosectioned (n = 4) Experiment was repeated independently with similar results. **e** Mice were injected I.V. with 0.5% Evans Blue. After 2 hours mice were perfused intraventricularly and EB was extracted from brain tissue using DMF (WT, LPS, AAV-VEGF-C, VEGF-C-mRNA, n = 4; Tumor, Tumor + VEGF-C-mRNA, n = 5). **f** Representative image of AAV-CTRL and AAV-VEGF-C treated mice after implantation of 5,000 cells. Experiment was repeated independently with similar results. **g** Long term survival monitoring of mice after AAV-VEGF-C and AAV-CTRL injections into the cisterna

magna (n = 5). **h-i** C57BL/6 mice received injection of AAV-CTRL or AAV-VEGF-C intracisternally (icm) through the cisterna magna. Six to eight weeks later, mice were euthanized and the dura was collected to image the lymphatic vasculature ($LYVE1^+$) in the superior sagittal sinus (AAV-CTRL, n = 4; AAV-VEGF-C, n = 5). **j** C57BL/6 mice injected with CTRL-AAV or AAV-VEGF-C icm two months prior were implanted with 50,000 GL261-Luc cells in the striatum and monitored for survival (AAV-CTRL, n = 4; AAV-VEGF-C, n = 5) or. **k** AAV-CTRL or AAV-VEGF-C treated mice were depleted of CD4 or CD8 T cells using anti-CD4 (GK1.5) or anti-CD8 (YTS169.4) antibodies starting one day before tumor inoculation (GL261) and re-dosed every four days after (**k**; AAV-CTRL, n = 4; AAV-VEGF-C, n = 5; AAV-VEGF-C + αCD8, n = 4; AAV-VEGF-C + αCD4, n = 5). **l** muMT, B cell deficient mice were injected with AAV-CTRL or AAV-VEGF-C and challenged with 50,000 GL261-Luc cells two months after (AAV-CTRL, n = 5; muMT AAV-CTRL, n = 3; muMT AAV-VEGF-C, n = 5). **m** Schematic of mice procedure schedule in Fig 1f and Extended Data Fig 1m. Mice injected with AAV-CTRL or AAV-VEGF-C that survived over 100 days after 5,000 GL261-Luc challenge were re-challenged with 500,000 GL261-Luc in the flank. **m** IVIS imaging of mice ten days after flank re-challenge, and measurement of tumors at day 7 and 15 (n = 3). Data are pooled from two independent experiments (**h-m**). Data are mean ± S.D. *P < 0.05; **P < 0.01; ***P <0.001; ****P<0.0001 (two-tailed unpaired Student's t-test, two-sided Log-rank Mantel-Cox test)

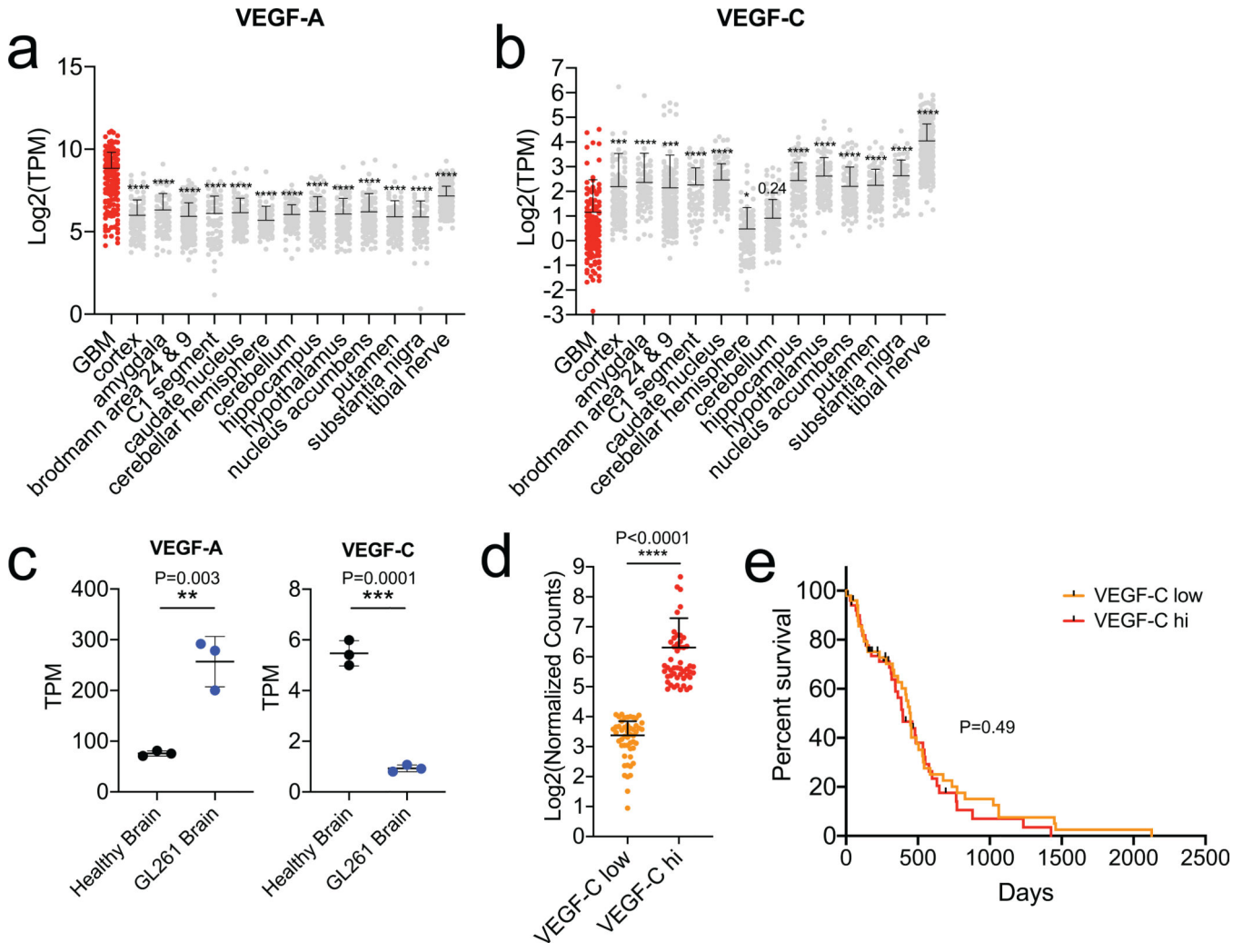

Extended Data Fig 2. Correlation of VEGF-C expression profiles between human and murine GBM.

a-c RNAseq data of tumor tissue and healthy brain tissue from different regions of the tissue (TCGA (phs000178.v10.p8) and GTEX respectively (v6). **a** Expression profile of VEGF-A. **b** Expression profile of VEGF-C (GBM, n = 147; cortex, n = 133; amygdala, n = 81; Brodmann area 24&9, n = 215; C1 segment, n = 75; caudate nucleus, n = 135; cerebellar hemisphere, n = 115; cerebellum, n = 146; hippocampus, n = 103; hypothalamus, n = 101; nucleus accumbens, n = 125; putamen, n = 103; substantia nigra, n = 72; tibial nerve, n = 329). **c** RNAseq data of mice brain and GL261 tumors from mice brains were analyzed (n = 3 biologically independent samples). **d** ONCLNC (Onclnc.org) data of GBM patients stratified into two groups (VEGF-C low, lower 33%; VEGF-C hi, upper 33%; n = 50). **e** Kaplan Meier Survival curve of patients from **e** (n = 50). Data are mean ± S.D. *P < 0.05; **P < 0.01; ***P <0.001; ****P<0.0001 (two-tailed unpaired Student's t-test, two-sided Log-rank Mantel-Cox test, Pearson's correlation)

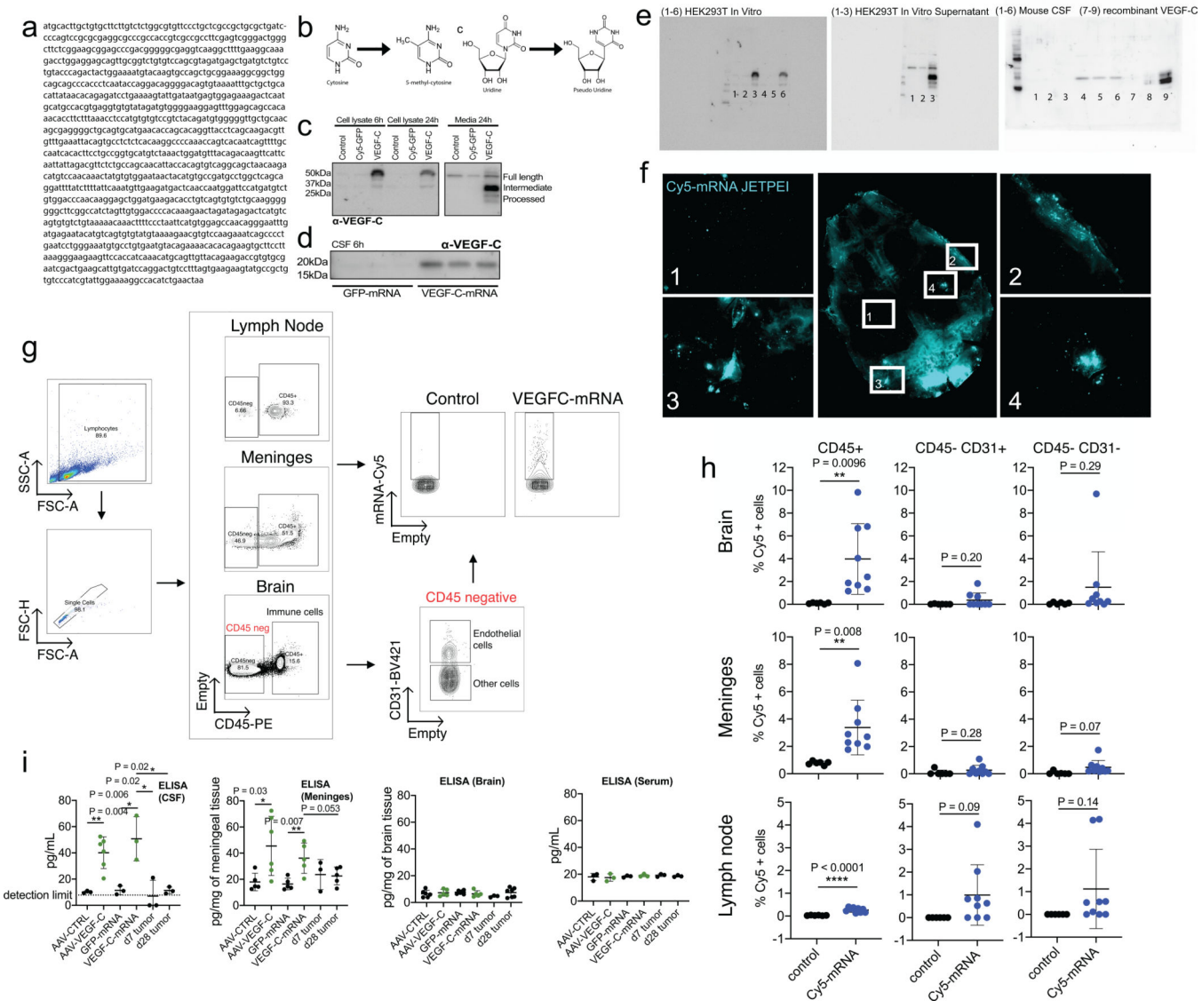

Extended Data Fig 3. VEGF-C-mRNA validation in vitro and in vivo uptake/expression tropism. **a** cDNA sequence of VEGF-C used for mRNA production. **b** 5-methyl cytosine and pseudo uridine were used to substitute all of cytosine and uridine in the mRNA. **c** VEGF-C-mRNA was transfected into HEK293T cells and cell lysate and media were collected to detect full length, and secreted intermediate and processed peptides. **d** VEGF-C-mRNA (5 μg) was delivered in vivo into the cisterna magna of mice using a JETPEI polyplex system. Six hours after, mice CSF was collected using a capillary tube, filtered with an amicon filter and the wash-through was used to run a western blot (each lane is n = 10 animals pooled). **e** Raw western blot images of Extended Data Fig 4c (gel 1: column 1, control; 2, Cy5-GFP-mRNA; 3, VEGF-C-mRNA; 4, control; 5, Cy5-GFP-mRNA; 6, VEGF-C-mRNA) (gel 2: column 1, control; 2, Cy5-GFP-mRNA; 3, VEGF-C-mRNA) and Extended Data Fig 4d (gel 3: column 1–3 Cy5-GFP-mRNA; column 4–6 Cy5-GFP-mRNA; 7–9 recombinant human VEGF-C in increasing concentration). Experiments were repeated twice independently with similar results. **f** VEGF-C-mRNA and Cy5 labeled GFP-mRNA was mixed at a 1:1 ratio and

delivered in vivo with JETPEI. 15 minutes later, mice were euthanized and whole skull cap was imaged to observe the distribution of mRNA particles. Experiments were repeated independently twice with similar results. **g-h**VEGF-C-mRNA and Cy5 labeled GFP-mRNA were mixed at a 1:1 ratio and delivered in vivo with JETPEI. 24 h later brains, meninges and lymph nodes of treated mice were collected for flow cytometry to measure % Cy5 positive cells in each compartment (control, n = 6; Cy5-mRNA, n = 9; data are pooled from two independent experiments). **i** CSF, Meninges, Brain and Serum were collected at 2 month-time point (AAV-CTRL, AAV-VEGF-C), 24 h-time point (GFP-mRNA, VEGF-C-mRNA), or days 7 and 28 after tumor inoculation and ELISA was performed to detect VEGF-C (CSF; AAV-VEGF-C, n = 6; other groups n = 3; 5 animals were pooled for each sample) (Meninges; AAV-VEGF-C, n = 6; d7 tumor, n =3; other groups n = 5). (Brain; AAV-CTRL, GFP-mRNA, n = 6; AAV-VEGF-C, VEGF-C-mRNA, n = 5; d7 tumor, n = 3; d28 tumor, n = 7) (Serum; n = 3). Data are mean ± S.D. *P < 0.05; **P < 0.01; ***P <0.001; ****P<0.0001 (two-tailed unpaired Student’s t-test)

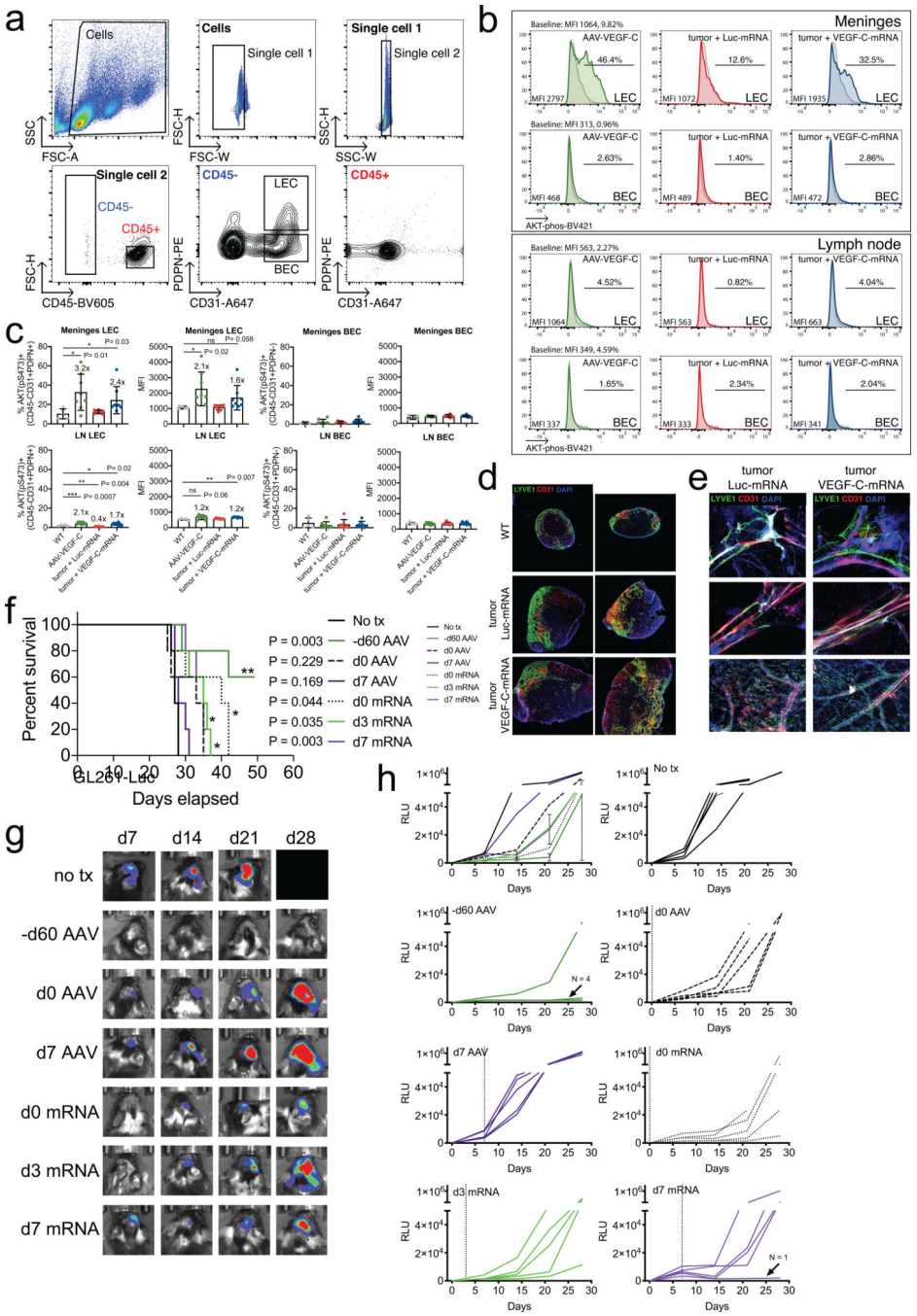

Extended Data Fig 4. VEGF-C signals specifically in lymphatic endothelial cells in the meninges and dCLNs and provides survival benefits in an administration timepoint dependent manner.

(**a**) Gating strategy for lymphatic endothelial cells (LECs) and blood endothelial cells (BECs). (**b**) Concatenated images of LECs and BECs from meninges and lymph node depicting AKT-phosphorylation intensity. Experiment was repeated independently with similar results. (**c**) Quantification of AKT(pS473) positive population and MFI within LECs and BECs in the meninges and dCLNs (meninges; WT, n = 5; AAV-VEGF-C, tumor + Luc-mRNA, tumor + VEGF-C-mRNA, n = 8) (lymph nodes; WT, n = 5; AAV-VEGF-C, n = 8;

tumor + Luc-mRNA, n = 7; tumor + VEGF-C-mRNA, n = 8). (**d**) Fluorescent microscope images of dCLN after VEGF-C-mRNA treatment in tumor bearing mice (CD31, red; LYVE1, green; DAPI, blue). (**e**) Fluorescent microscope images of meninges after VEGF-C-mRNA treatment in tumor bearing mice (CD31, red; LYVE1, green; DAPI, blue). Experiment was repeated independently with similar results. **f-h** Mice were treated with AAV-VEGF-C or VEGF-C-mRNA at different timepoints relative to GL261-Luc tumor inoculation (d0). Tumor growth kinetics (**g-h**) and survival (**f**) was monitored (n = 5 for all groups). *P < 0.05; **P < 0.01; ***P <0.001; ****P<0.0001 (two-sided Log-rank Mantel-Cox test). Data are mean ± S.D. *P < 0.05; **P < 0.01; ***P <0.001; ****P<0.0001 (two-tailed unpaired Student's t-test)

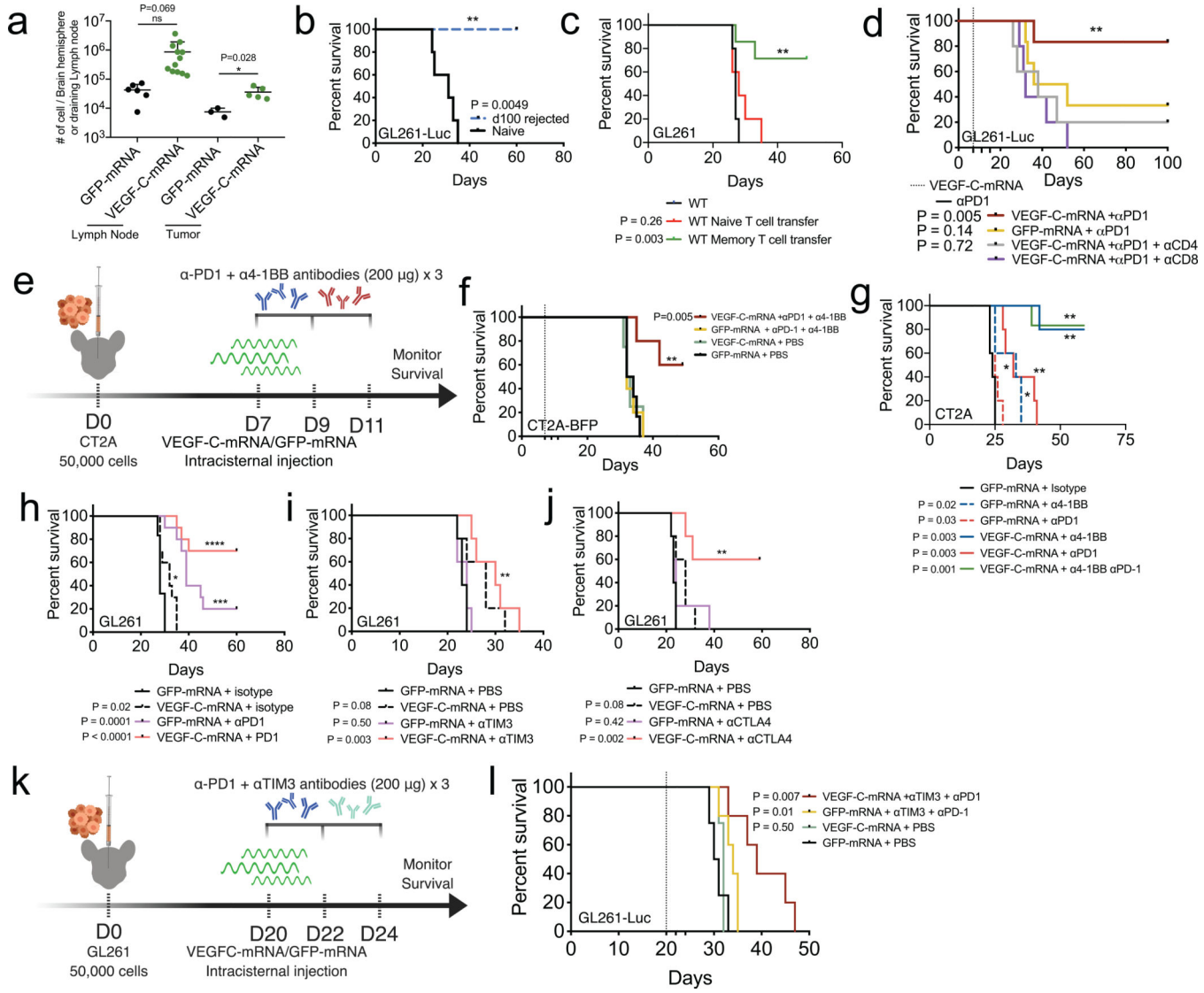

Extended Data Fig 5. Therapeutic delivery of VEGF-C potentiates checkpoint inhibitor therapy even at late stages of tumor development.

a (Fig 3c–d) Cell number quantification per tumor of bearing hemisphere or lymph node using CountBright absolute beads and autocounter (see methods for details) (Lymph node; GFP-mRNA n = 6; VEGF-C-mRNA, n = 12) (Tumor; GFP-mRNA n = 3; VEGF-C-mRNA, n = 5). **b** Mice that rejected tumors after VEGF-C-mRNA + anti-PD1 (RMP1–14) combination therapy were re-challenged in the contralateral hemisphere and observed for survival (Naïve, n = 5; d100 rejected, n = 4). **c** T cells from lymph nodes and spleens from mice that rejected tumors after VEGF-C-mRNA + anti-PD1 (RMP1–14) combination therapy or naïve WT mice were isolated and transferred into naïve WT mice intravenously. 24 h later, GL261 tumors were inoculated intracranially and observed for survival (WT, n = 5; WT Naïve T cell transfer, n = 5; WT Memory T cell transfer, n = 7). **d** Mice inoculated with 50,000 GL261-Luc cells were treated with VEGF-C-mRNA/GFP-mRNA (day 7) and with either anti-PD1 (RMP1–14) antibodies or isotype antibodies (day 7, 9 and 11) and monitored for survival. Mice were depleted of CD4 or CD8 T cells using anti-CD4 (GK1.5)

or anti-CD8 (YTS169.4) antibodies starting one day before tumor inoculation and re-dosed every four days after (VEGF-C-mRNA + αPD-1, n = 6; GFP-mRNA + αPD-1, n = 6; VEGF-C-mRNA + αPD-1 + αCD4, n = 5; VEGF-C-mRNA + αPD-1 + αCD8, n = 5). **e** Schematic for experiment design of **f-g**. **f-g** Mice inoculated with 50,000 CT2A-BFP cells (**f**) or CT2A cells (**g**) were treated with VEGF-C-mRNA/GFP-mRNA (day 7) and with either anti-PD1(RMP1–14) and/or anti-4–1BB (LOB12.3) antibodies or PBS (day 7, 9 and 11) and monitored for survival (**f** VEGF-C-mRNA + αPD1 + α4–1BB, n = 5; GFP-mRNA + αPD1 + α4–1BB, n = 5; VEGF-C-mRNA + PBS, n = 4; GFP-mRNA + PBS, n = 6) (**g** n = 5 for all groups except VEGF-C-mRNA + α4–1BB αPD1, n = 7). **h-j** Mice inoculated with 50,000 GL261 cells were treated with VEGF-C-mRNA/GFP-mRNA (day 7) and with either anti-PD1 (RMP1–14) antibodies (**h**), anti-TIM3 (RMT3–23) antibodies (**i**), anti-CTLA4 (9H10) antibodies (**j**) or PBS (day 7, 9 and 11) and monitored for survival (n = 5). For **i** and **j** same control mice were used for GFP-mRNA + PBS and VEGF-C-mRNA + PBS groups. **k** Schematic for experiment design of **l**. **l** Mice inoculated with 50,000 GL261-Luc cells were treated with VEGF-C-mRNA/GFP-mRNA (day 20) and with either anti-PD1 (RMP1–14) and anti-TIM3 (RMT3–23) antibodies or PBS (day 20, 22, 24) and monitored for survival (n = 5). *P < 0.05; **P < 0.01; ***P <0.001; ****P<0.0001 (two-tailed unpaired Student’s t-test, two-sided Log-rank Mantel-Cox test)

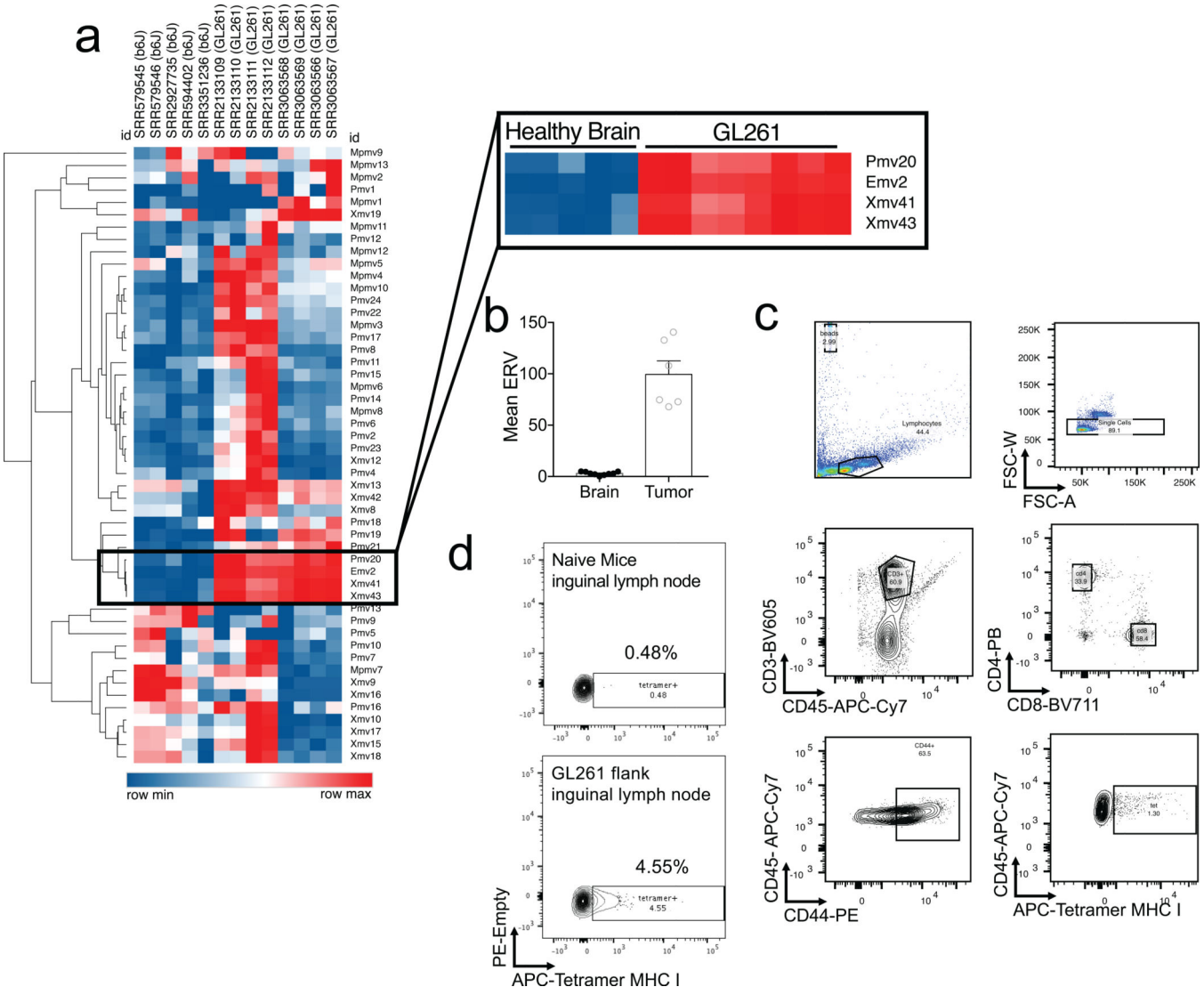

Extended Data Fig 6. Validation of endogenous retrovirus EMV2 as a tumor antigen for GL261.

a RNA-seq analysis of murine endogenous retrovirus elements in publicly available data sets on C57BL/6J mice brains and GL261 cell lines from various sources. **b** Quantification of ERV elements in brain and tumor tissue from RNA-Seq (Brain, n = 9; Tumor, n = 6). **c** Gating strategies for tetramer staining. **d** Mice were injected with 500,000 GL261 cells or PBS in the flank. Seven days after tumor inoculation, draining inguinal lymph nodes were collected and emv2-env (K^b-restricted peptides aa 604–611 of p15E protein (KSPWFTTL)) tetramers were used to validate tumor specific T cell proliferation. Experiments were repeated twice independently with similar results. Data are mean ± S.E.M

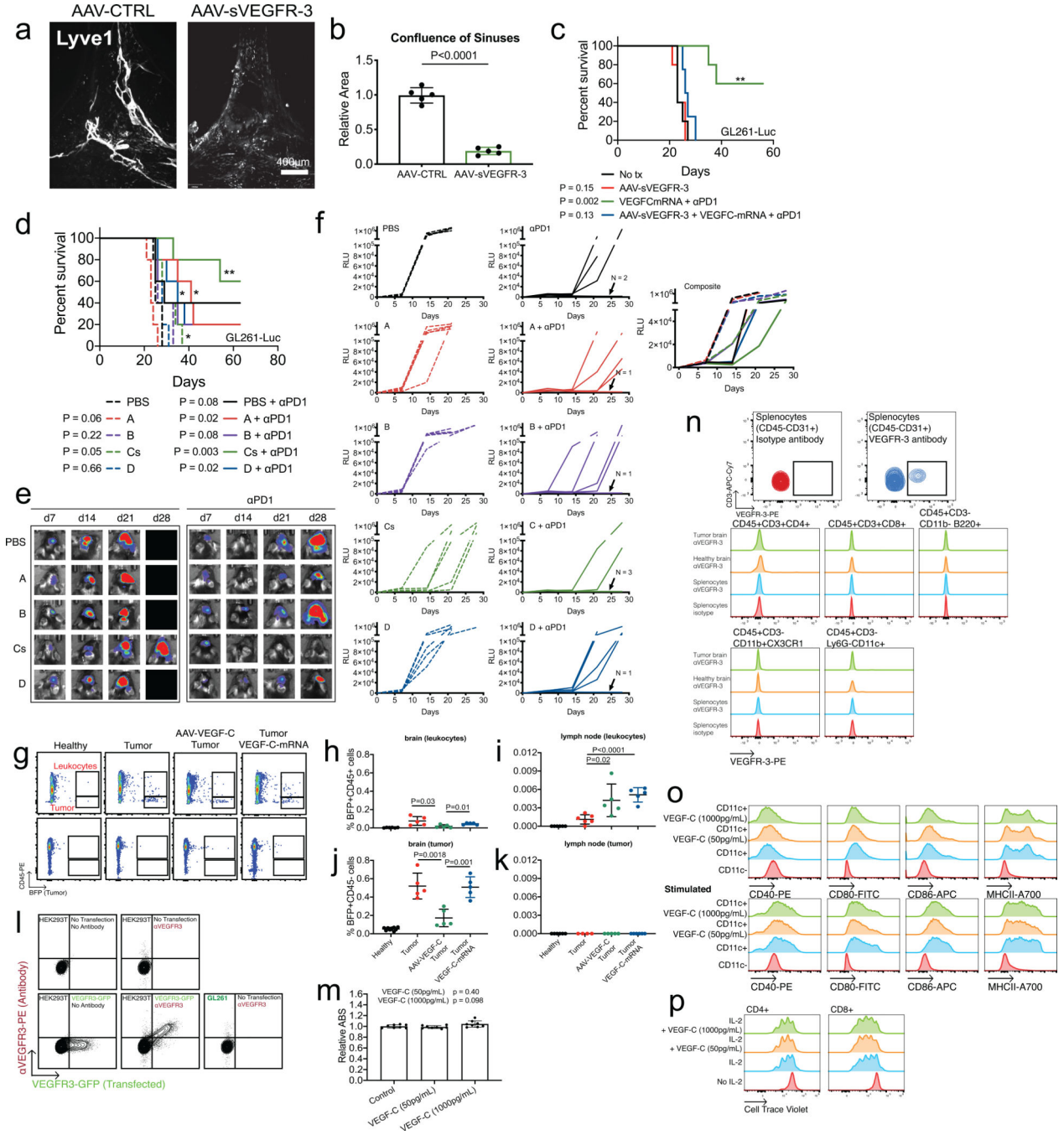

Extended Data Fig 7. VEGF-C dependent anti-PD-1 potentiation is specific among other VEGF family proteins and is not through a direct effect on tumor or immune cells.

a C57BL/6 mice received intra-cisterna magna (icm) injection of AAV-CTRL or -sVEGFR-3. After 4 weeks, mice were euthanized and the dura mater was collected to image the lymphatic vasculature (LYVE1) in the confluence of sinuses (**b**) (n = 5). **c** Mice were pre-treated with AAV-sVEGFR-3 4–6 weeks prior to tumor inoculation. 7 days post tumor inoculation, mice were treated with VEGF-C-mRNA and anti-PD1 (RMP1–14) antibodies (days 7, 9 and 11) (n = 5). **d-f** Mice were treated with 5 μg of recombinant protein (VEGF-

A, B, C156S, or D) in combination with anti-PD1 (RMP1–14) antibodies (days 7, 9 and 11) and monitored for survival (n = 5). **g-k** Mice were injected with CT2A-BFP tumors. Mice were treated with VEGF-C-mRNA at day 7. On day 8, brains and lymph nodes from all mice were collected and analyzed using flow cytometry. Experiment was repeated independently with similar results. **g** Sample plots of experiments, **h-k** quantification of experiments (n = 5). **l** Flow cytometry was used to evaluate VEGFR-3 expression in GL261 cells. VEGFR3-GFP plasmid was transfected into HEK293T cells as a positive control. Experiment was repeated independently with similar results. **m** MTT assay to measure GL261 cancer cell proliferation in the presence of VEGF-C after 48 hours (all groups, n = 8). **n** Flow cytometry was used to evaluate VEGFR-3 expression in leukocyte compartments in the tumor. Experiment was repeated independently with similar results. **o** BMDCs were cultured with VEGF-C and evaluated for costimulatory molecule expression at naïve state (top row) or with LPS stimulation (bottom row). **p** Isolated T cells were activated *in vitro* with CD3/CD28 and IL-2 in the presence of VEGF-C. Data are mean ± S.D. *P < 0.05; **P < 0.01; ***P <0.001; ****P<0.0001 (two-tailed unpaired Student's t-test, two-sided Log-rank Mantel-Cox test).

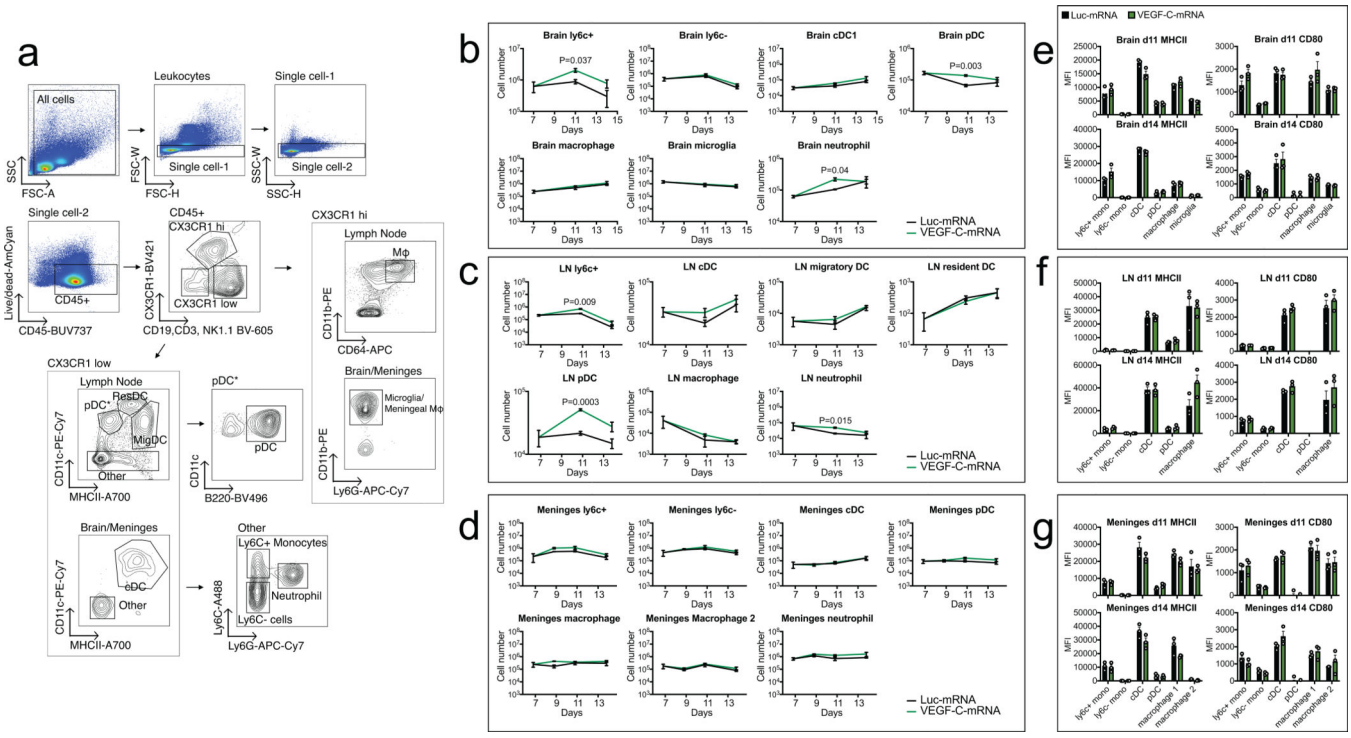

Extended Data Fig 8. Flow cytometry analysis of myeloid cell populations after VEGF-C treatment.

Mice bearing 7 day-tumors were treated with Luc-mRNA or VEGF-C-mRNA and evaluated for changes in myeloid populations. **a** Gating strategy for different myeloid cells. **b-d** Cell counts of different cell types were measured at different time points after VEGF-C-mRNA treatment. **e-g** MHCII and CD80 MFI levels were graphed and showed no significant alteration after VEGF-C-mRNA treatment. **b** and **e** are leukocytes from brain tissue. **c** and **f** are leukocytes from draining cervical lymph nodes. **d** and **g** are leukocytes from meninges (n = 3, 3 animals pooled for each replicate). Data are mean ± S.E.M *P < 0.05; **P < 0.01; ***P <0.001; ****P<0.0001 (two-tailed unpaired Student's t-test)

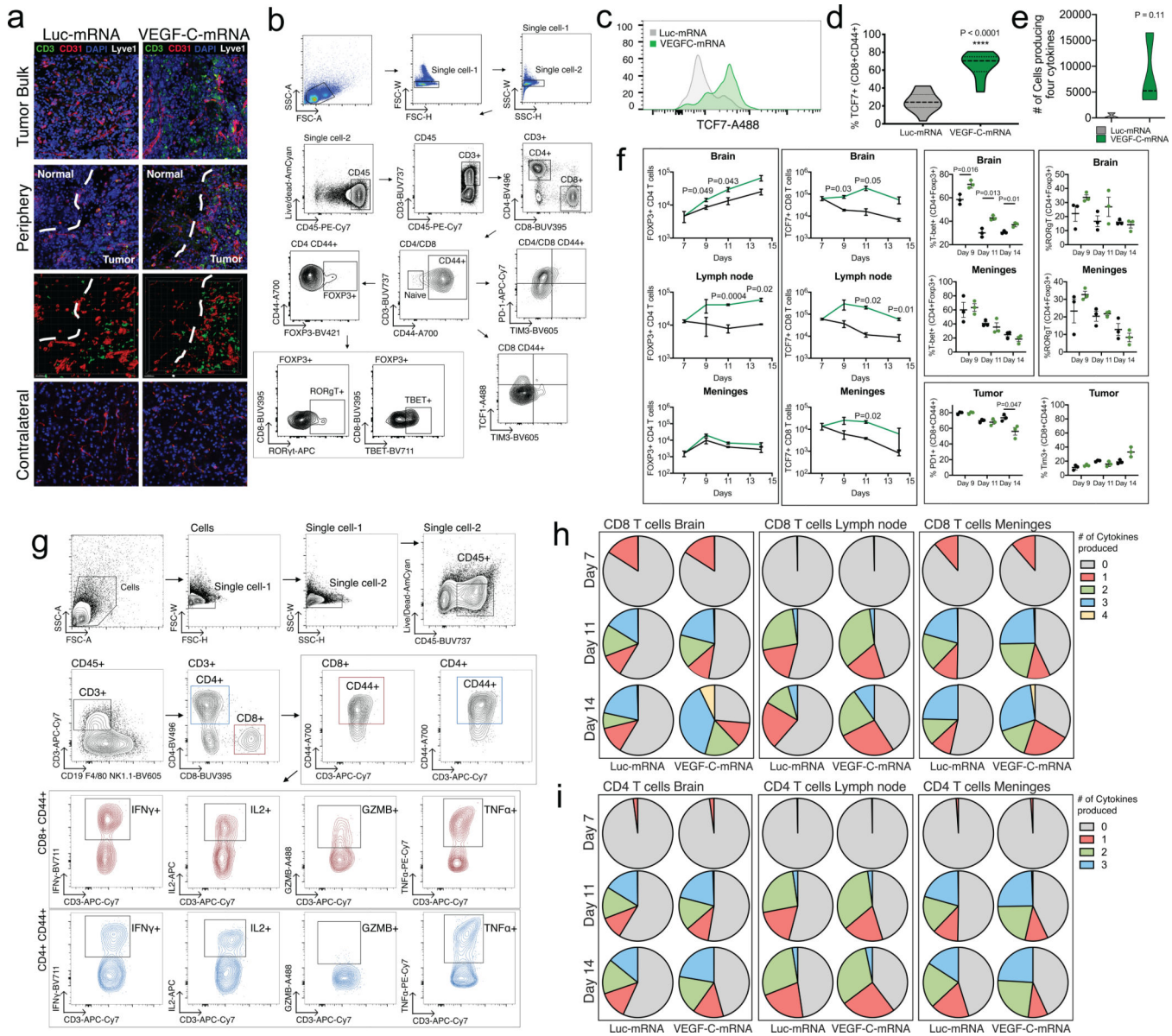

Extended Data Fig 9. VEGF-C treatment changes T cell phenotypes and functionality.

Mice bearing 7 day-tumors were treated with Luc-mRNA or VEGF-C-mRNA and evaluated for changes. **a** Mice brains were collected 2 days after VEGF-C-mRNA treatment, cryosectioned and analyzed by immunofluorescence microscopy. **b** Gating strategy for flow cytometry analysis of T cells. **c** Example of TCF7 staining in $CD3^+CD8^+CD44^+$ populations after VEGF-C-mRNA treatment. Experiment was repeated twice independently with similar results. **d** Percent of TCF7+ T cells in $CD3^+CD8^+CD44^+$ population in the brain (Luc-mRNA, n = 14; VEGF-C-mRNA, n = 9, data pooled from 3 independent experiments). **e** Number of cells $CD3^+CD8^+CD44^+$ cells producing IFNγ, TNFα, IL2 and GZMB in the brain (n = 3; 3 animals were pooled for each n). Violin plots display quartiles with dotted horizontal lines, median with dashed lines and minima and maxima with solid lines. **f** Quantification of cell counts in different compartments after VEGF-C-mRNA treatment.

Percent of cells expressing specific transcription factors or immune checkpoint inhibitors after VEGF-C-mRNA treatment. **g** Gating strategy for cytokine production in T cells. **h-i** Quantification of T cells expressing multiple cytokines (n = 3, 3 animals pooled for each replicate). Data are mean ± S.E.M *P < 0.05; **P < 0.01; ***P <0.001; ****P<0.0001 (two-tailed unpaired Student's t-test)

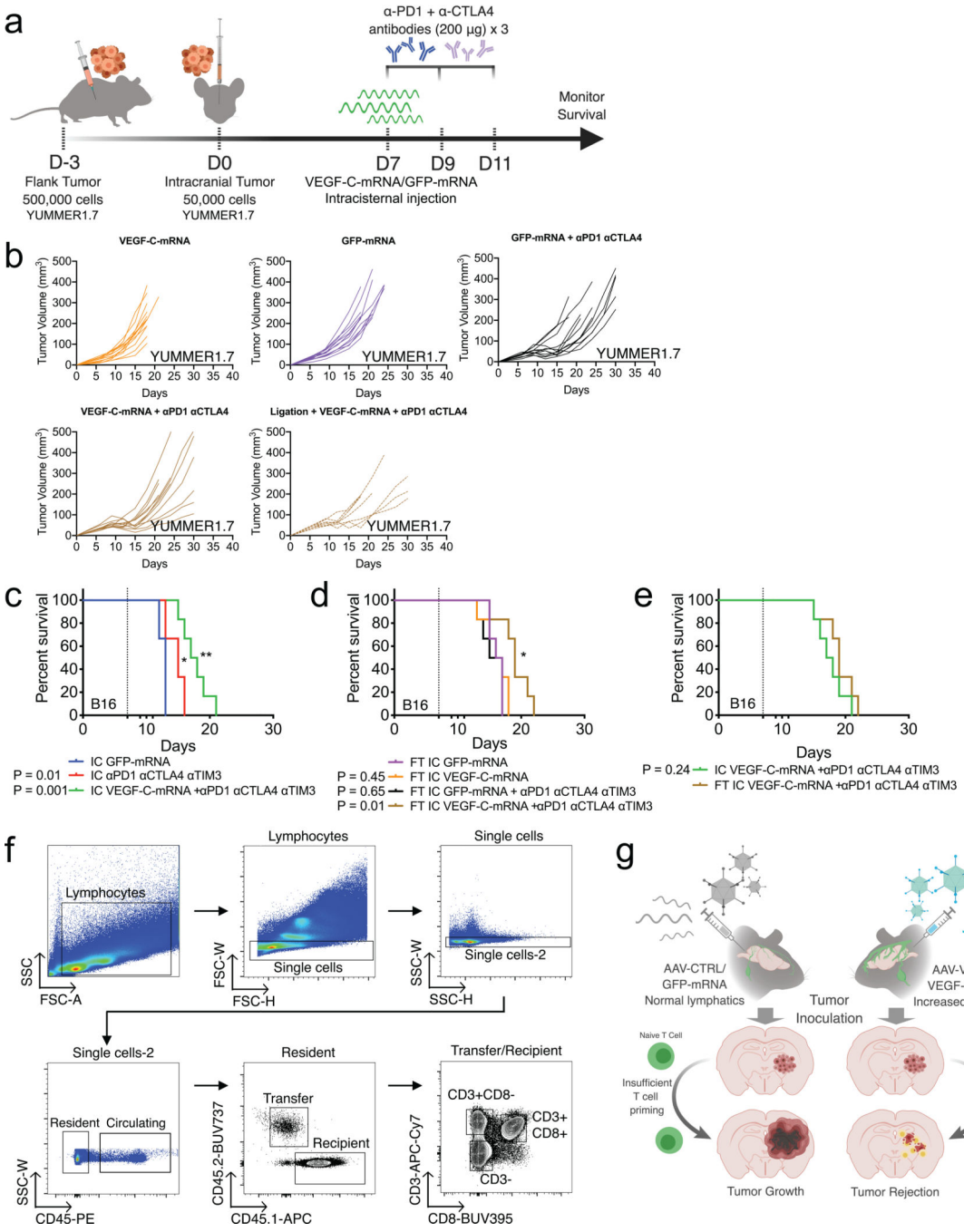

Extended Data Fig 10. T cell extrinsic VEGF-C signaling mediates protection against intracranial tumor and is equivalent to peripheral priming.

a Schematic of experiment design for main Fig **a-c** and Extended Fig. 13a-e. **b** Flank tumor growth kinetics from main Fig 4a–c were measured using a caliper (n = 12 for all groups except; ligation groups, n = 7). **c-e** mice were given either only intracranial B16 tumors (IC, **c**) or a B16 flank tumor and intracranial tumor (FT, **d**) and treated with GFP/VEGF-C-mRNA on day 7 and anti-PD1 (RMP1–14), anti-CTLA4 (9H10), and anti-TIM3 (RMT3–23) on days 7, 9 and 11. **f** Flow cytometry gating strategy for main Fig 4e–f. **g** Schematic of

VEGF-C induced tumor rejection. *P < 0.05; **P < 0.01; ***P <0.001; ****P<0.0001 (two-sided Log-rank Mantel-Cox test)

Supplementary Material

Refer to Web version on PubMed Central for supplementary material.

Acknowledgements

We thank members of the Iwasaki lab for insightful discussions and help with protocols. We thank Dr. Mark Saltzman (Yale BME) for allowing us to use mice stereotaxic equipment and help with materials. We thank S. Lee from the Thomas lab for initial help in breeding animals and the ICM Vectorology platform for AAV material production. This study was supported by awards from National Institute of Health grants, T32GM007205 (MSTP training grant) and F30CA239444 (to E.S.), AI054359 and AI127429 (to A.I.), R01EB016629–01 and R01 EY025979–01 (to J.L.T.), CA196660, CA128814, and CA121974 (to M.B.). A.I. is an investigator of the Howard Hughes Medical Institute. L.B. and J.L.T. were supported by the Yale School of Medicine. Work in the Alitalo lab was funded by the iCAN Digital Precision Cancer Medicine Flagship, Academy of Finland (grants nos. 292816 and 273817, 307366, Centre of Excellence Program 2014–2019, Cancer Foundation in Finland, Sigrid Juselius Foundation, Hospital District of Helsinki and Uusimaa Research Grants, Helsinki Institute of Life Sciences (HiLIFE), Biocenter Finland (to K.A.)

References

1. Aspelund A et al. A dural lymphatic vascular system that drains brain interstitial fluid and macromolecules. J Exp Med 212, 991–999, doi:10.1084/jem.20142290 (2015). [PubMed: 26077718]
2. Louveau A et al. Structural and functional features of central nervous system lymphatic vessels. Nature 523, 337–341, doi:10.1038/nature14432 (2015). [PubMed: 26030524]
3. Louveau A et al. CNS lymphatic drainage and neuroinflammation are regulated by meningeal lymphatic vasculature. Nat Neurosci 21, 1380–1391, doi:10.1038/s41593-018-0227-9 (2018). [PubMed: 30224810]
4. Antila S et al. Development and plasticity of meningeal lymphatic vessels. J Exp Med 214, 3645–3667, doi:10.1084/jem.20170391 (2017). [PubMed: 29141865]
5. Da Mesquita S et al. Functional aspects of meningeal lymphatics in ageing and Alzheimer's disease. Nature, doi:10.1038/s41586-018-0368-8 (2018).
6. Harris MG et al. Immune privilege of the CNS is not the consequence of limited antigen sampling. Sci Rep 4, 4422, doi:10.1038/srep04422 (2014). [PubMed: 24651727]
7. Mathieu E, Gupta N, Macdonald RL, Ai J & Yucel YH In vivo imaging of lymphatic drainage of cerebrospinal fluid in mouse. Fluids Barriers CNS 10, 35, doi:10.1186/2045-8118-10-35 (2013). [PubMed: 24360130]
8. Fankhauser M et al. Tumor lymphangiogenesis promotes T cell infiltration and potentiates immunotherapy in melanoma. Sci Transl Med 9, doi:10.1126/scitranslmed.aal4712 (2017).
9. Skobe M et al. Induction of tumor lymphangiogenesis by VEGF-C promotes breast cancer metastasis. Nat Med 7, 192–198, doi:10.1038/84643 (2001). [PubMed: 11175850]
10. Gilbert MR et al. A randomized trial of bevacizumab for newly diagnosed glioblastoma. N Engl J Med 370, 699–708, doi:10.1056/NEJMoa1308573 (2014). [PubMed: 24552317]
11. Cloughesy TF et al. Neoadjuvant anti-PD-1 immunotherapy promotes a survival benefit with intratumoral and systemic immune responses in recurrent glioblastoma. Nat Med 25, 477–486, doi:10.1038/s41591-018-0337-7 (2019). [PubMed: 30742122]
12. Mingozzi F & High KA Immune responses to AAV vectors: overcoming barriers to successful gene therapy. Blood 122, 23–36, doi:10.1182/blood-2013-01-306647 (2013). [PubMed: 23596044]
13. Sabnis S et al. A Novel Amino Lipid Series for mRNA Delivery: Improved Endosomal Escape and Sustained Pharmacology and Safety in Non-human Primates. Mol Ther 26, 1509–1519, doi:10.1016/j.ymthe.2018.03.010 (2018). [PubMed: 29653760]

14. Joukov V et al. Proteolytic processing regulates receptor specificity and activity of VEGF-C. EMBO J 16, 3898–3911, doi:10.1093/emboj/16.13.3898 (1997). [PubMed: 9233800]
15. Zincarelli C, Soltys S, Rengo G & Rabinowitz JE Analysis of AAV serotypes 1–9 mediated gene expression and tropism in mice after systemic injection. Mol Ther 16, 1073–1080, doi:10.1038/mt.2008.76 (2008). [PubMed: 18414476]
16. Zeng J et al. Anti-PD-1 blockade and stereotactic radiation produce long-term survival in mice with intracranial gliomas. Int J Radiat Oncol Biol Phys 86, 343–349, doi:10.1016/j.ijrobp.2012.12.025 (2013). [PubMed: 23462419]
17. Kim JE et al. Combination Therapy with Anti-PD-1, Anti-TIM-3, and Focal Radiation Results in Regression of Murine Gliomas. Clin Cancer Res 23, 124–136, doi:10.1158/1078-0432.CCR-15-1535 (2017). [PubMed: 27358487]
18. Filley AC, Henriquez M & Dey M Recurrent glioma clinical trial, CheckMate-143: the game is not over yet. Oncotarget 8, 91779–91794, doi:10.18632/oncotarget.21586 (2017). [PubMed: 29207684]
19. Garzon-Muvdi T et al. Dendritic cell activation enhances anti-PD-1 mediated immunotherapy against glioblastoma. Oncotarget 9, 20681–20697, doi:10.18632/oncotarget.25061 (2018). [PubMed: 29755681]
20. Chongsathidkiet P et al. Sequestration of T cells in bone marrow in the setting of glioblastoma and other intracranial tumors. Nat Med 24, 1459–1468, doi:10.1038/s41591-018-0135-2 (2018). [PubMed: 30104766]
21. Belcaid Z et al. Focal radiation therapy combined with 4–1BB activation and CTLA-4 blockade yields long-term survival and a protective antigen-specific memory response in a murine glioma model. PLoS One 9, e101764, doi:10.1371/journal.pone.0101764 (2014). [PubMed: 25013914]
22. Bronte V et al. Effective genetic vaccination with a widely shared endogenous retroviral tumor antigen requires CD40 stimulation during tumor rejection phase. J Immunol 171, 6396–6405 (2003). [PubMed: 14662838]
23. Rooney MS, Shukla SA, Wu CJ, Getz G & Hacohen N Molecular and genetic properties of tumors associated with local immune cytolytic activity. Cell 160, 48–61, doi:10.1016/j.cell.2014.12.033 (2015). [PubMed: 25594174]
24. He Y et al. Vascular endothelial cell growth factor receptor 3-mediated activation of lymphatic endothelium is crucial for tumor cell entry and spread via lymphatic vessels. Cancer Res 65, 4739–4746, doi:10.1158/0008-5472.CAN-04-4576 (2005). [PubMed: 15930292]
25. Hirakawa S et al. VEGF-C-induced lymphangiogenesis in sentinel lymph nodes promotes tumor metastasis to distant sites. Blood 109, 1010–1017, doi:10.1182/blood-2006-05-021758 (2007). [PubMed: 17032920]
26. Im SJ et al. Defining CD8+ T cells that provide the proliferative burst after PD-1 therapy. Nature 537, 417–421, doi:10.1038/nature19330 (2016). [PubMed: 27501248]
27. Siddiqui I et al. Intratumoral Tcf1(+)PD-1(+)CD8(+) T Cells with Stem-like Properties Promote Tumor Control in Response to Vaccination and Checkpoint Blockade Immunotherapy. Immunity 50, 195–211 e110, doi:10.1016/j.immuni.2018.12.021 (2019). [PubMed: 30635237]
28. Lucca LE et al. TIGIT signaling restores suppressor function of Th1 Tregs. JCI Insight 4, doi:10.1172/jci.insight.124427 (2019).
29. Huang AC et al. T-cell invigoration to tumour burden ratio associated with anti-PD-1 response. Nature 545, 60–65, doi:10.1038/nature22079 (2017). [PubMed: 28397821]
30. Tawbi HA et al. Combined Nivolumab and Ipilimumab in Melanoma Metastatic to the Brain. N Engl J Med 379, 722–730, doi:10.1056/NEJMoa1805453 (2018). [PubMed: 30134131]
31. Taggart D et al. Anti-PD-1/anti-CTLA-4 efficacy in melanoma brain metastases depends on extracranial disease and augmentation of CD8(+) T cell trafficking. Proc Natl Acad Sci U S A 115, E1540–E1549, doi:10.1073/pnas.1714089115 (2018). [PubMed: 29386395]
32. Medawar PB Immunity to Homologous Grafted Skin. III. The Fate of Skin Homografts Transplanted to the Brain, to Subcutaneous Tissue, and to the Anterior Chamber of the Eye. Br J Exp Pathol (1947).

33. Volovitz I et al. Split immunity: immune inhibition of rat gliomas by subcutaneous exposure to unmodified live tumor cells. J Immunol 187, 5452–5462, doi:10.4049/jimmunol.1003946 (2011). [PubMed: 21998458]

34. Breslin JW et al. Vascular endothelial growth factor-C stimulates the lymphatic pump by a VEGF receptor-3-dependent mechanism. Am J Physiol Heart Circ Physiol 293, H709–718, doi:10.1152/ajpheart.00102.2007 (2007). [PubMed: 17400713]

35. Wang J et al. UV-induced somatic mutations elicit a functional T cell response in the YUMMER1.7 mouse melanoma model. Pigment Cell Melanoma Res 30, 428–435, doi:10.1111/pcmr.12591 (2017). [PubMed: 28379630]

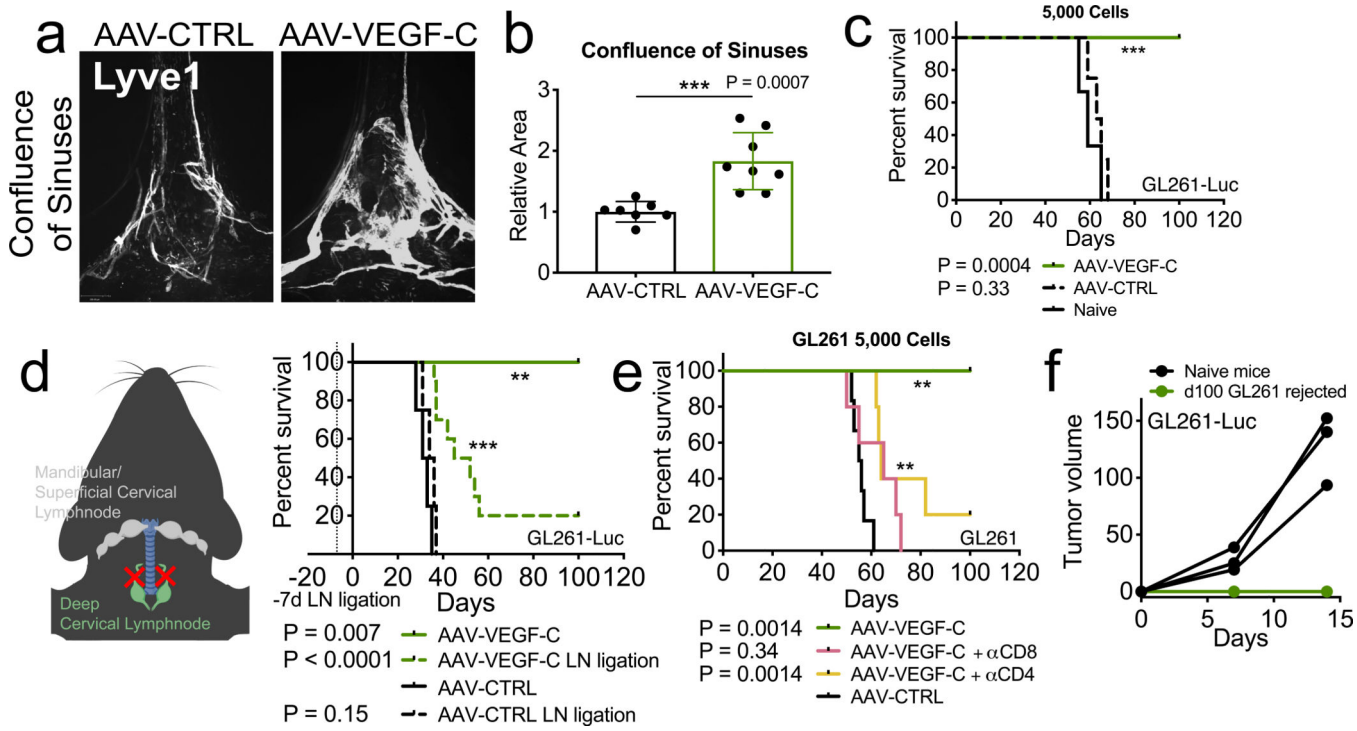

Figure 1. Increased meningeal lymphatic vasculature confers protection against intracranial glioblastoma challenge in a draining lymph node and T cell dependent manner and provides long-term protection.

a-b C57BL/6 mice received injection of AAV-CTRL or AAV-VEGF-C intra-cisternally (icm) through the cisterna magna. Six to eight weeks later, mice were euthanized and the dura was collected to image the lymphatic vasculature ($LYVE1^+$) in the confluence of sinuses (AAV-CTRL, n = 7; AAV-VEGF-C, n = 8). **c-e** C57BL/6 mice injected with CTRL-AAV or AAV-VEGF-C icm two months prior were implanted with 5,000 (**e**) (Naïve = 3, AAV-CTRL, n = 4; AAV-VEGF-C, n = 8) GL261-Luc cells in the striatum and monitored for survival. **d** Six to eight weeks after AAV icm injection, the dcLNs of mice were ligated using a cauterizer. Seven days later, mice were challenged with 50,000 GL261-Luc cells in the striatum and monitored for survival (AAV-CTRL, n = 4; AAV-CTRL LN ligation, n = 4; AAV-VEGF-C, n = 4; AAV-VEGF-C LN ligation, n = 10). **f** Mice injected with AAV-CTRL or AAV-VEGF-C that survived over 100 days after 5,000 GL261-Luc challenge were re-challenged with 500,000 GL261-Luc in the flank. IVIS imaging of mice ten days after flank re-challenge, and measurement of tumors at day 7 and 15 (n = 3). Data are pooled from two independent experiments (**b-f**). Data are mean ± S.D. *P < 0.05; **P < 0.01; ***P <0.001; ****P<0.0001 (two-tailed unpaired Student's t-test, two-sided Log-rank Mantel-Cox test)

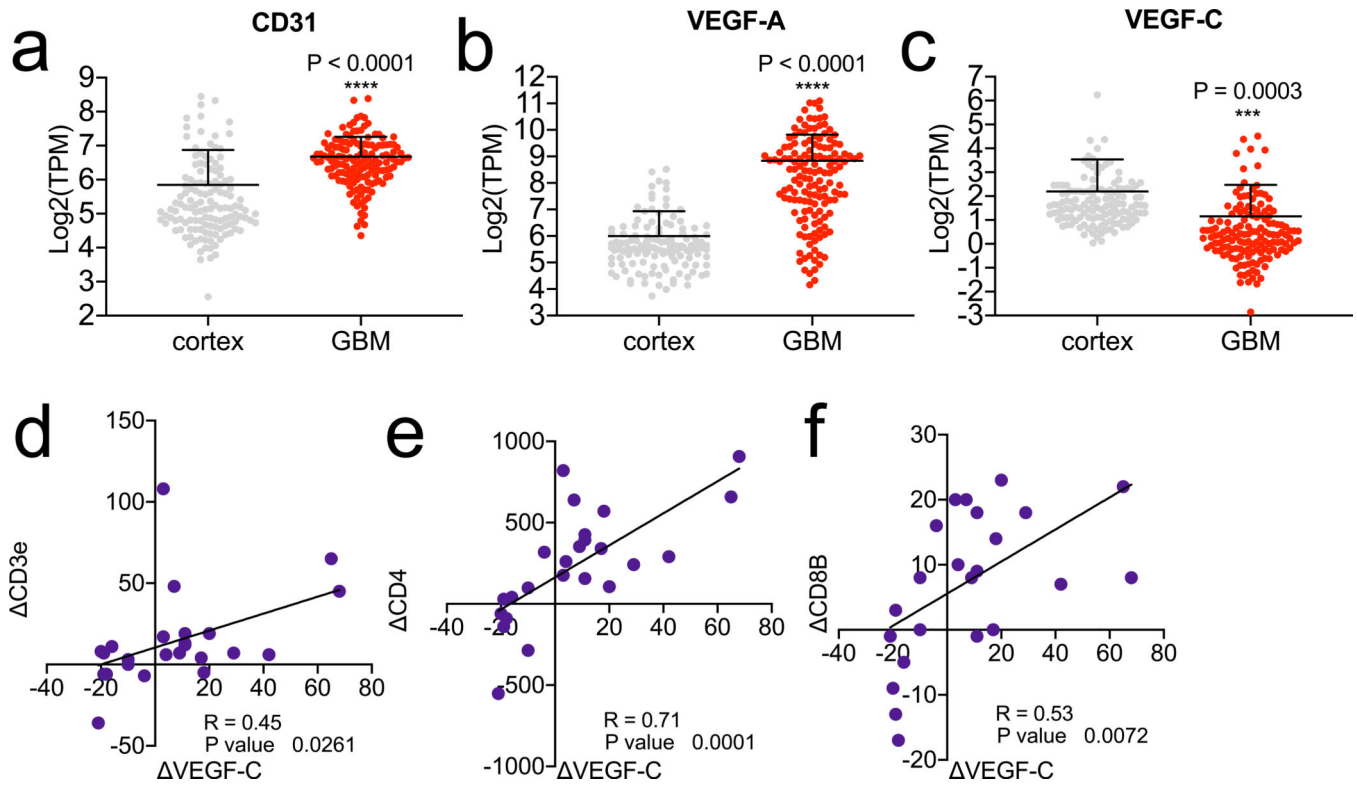

Figure 2. Human GBM is deprived of lymphangiogenic signals at steady state but increases after αPD-1 therapy.

RNAseq data of tumor tissue (TCGA, phs000178.v10.p8) and healthy brain cortex (GTEX, phs000424.v7.p2). **a-c** Expression profiles of VEGF-A, CD31 (angiogenic) and VEGF-C (lymphangiogenic) genes in cortex versus GBM samples (cortex, n = 133; GBM, n = 147, patient samples). **d-f** RNAseq correlation of change in VEGF-C and T cell markers after PD-1 therapy (data from GSE121810, n = 24). Data are mean ± S.D. *P < 0.05; **P < 0.01; ***P <0.001; ****P<0.0001 (two-tailed unpaired Student's t-test, Pearson's correlation)

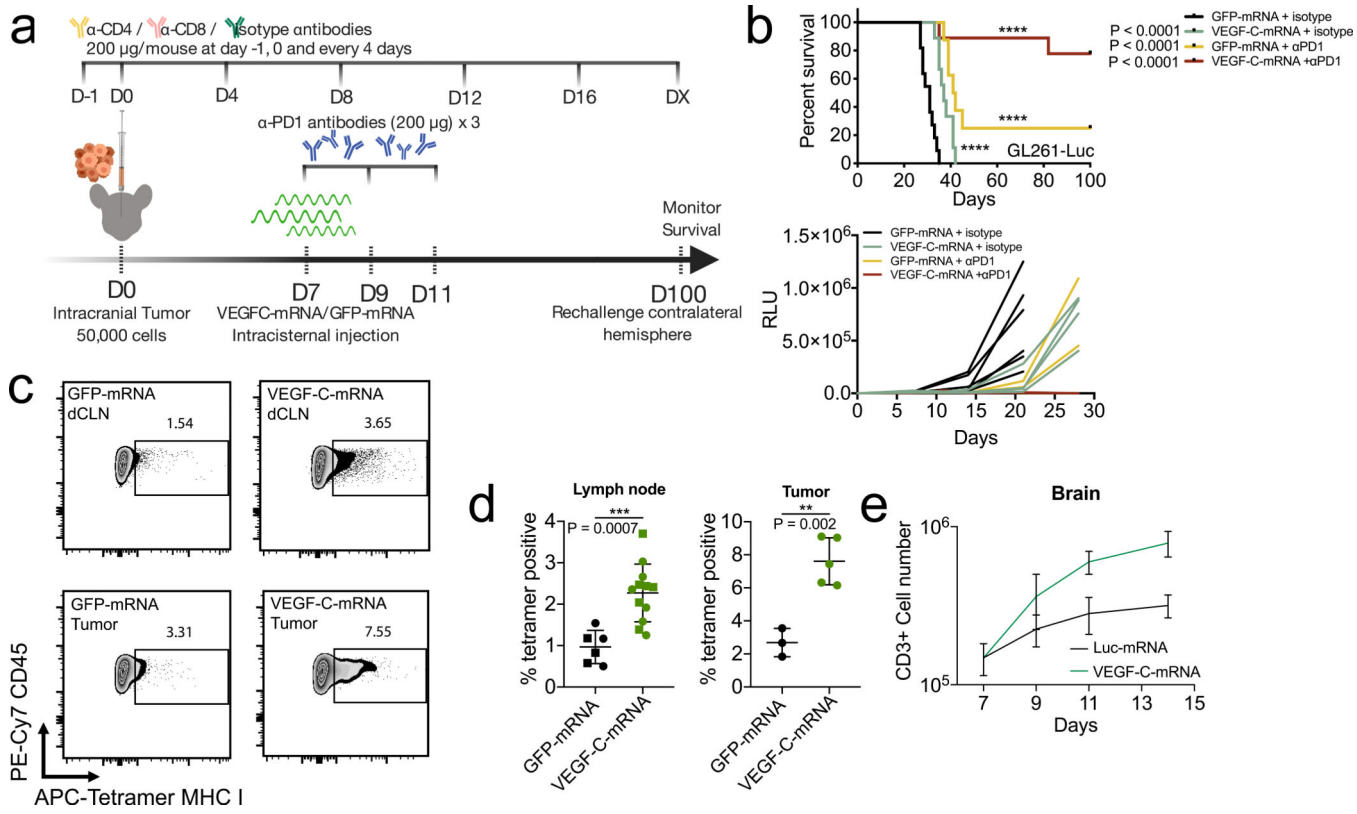

Figure 3. Therapeutic delivery of VEGF-C potentiates checkpoint inhibitor therapy by increased T cell priming.

a Schematic of treatment plans for (**b**). **b** Mice inoculated with 50,000 GL261-Luc cells were treated with VEGF-C-mRNA/GFP-mRNA (day 7) with either anti-PD1 (RMP1–14) antibodies or isotype antibodies (day 7, 9 and 11) and monitored for survival (kaplan meier curve; GFP-mRNA + isotype, n = 11; VEGF-C-mRNA + isotype, n = 9; GFP-mRNA + αPD1, n = 8; VEGF-C-mRNA + αPD1, n = 10, Data are pooled from 2 independent experiments) (tumor burden measurement; GFP-mRNA + isotype, n = 7; VEGF-C-mRNA + isotype, n = 5; GFP-mRNA + αPD1, n = 4; VEGF-C-mRNA + αPD1, n = 5). **c-d** Mice were inoculated with 50,000 GL261-Luc cells and treated with GFP-mRNA or VEGF-C-mRNA at day 7. Seven days after mRNA treatment, dcLNs and tumor bearing-brain hemisphere were collected to detect tetramer positive CD8 T cells. **c** Concatenated FACS plot of $CD45^+CD3^+CD8^+CD44^+$ T cells in tumor-bearing brain and dcLNs with GFP-mRNA or VEGF-C-mRNA treatment. Percent quantification of dcLNs (**d,** circle, ipsilateral; square, contralateral) or tumor infiltrating-tetramer positive CD8 T cells (Lymph node; GFP-mRNA n = 6; VEGF-C-mRNA, n = 12) (Tumor; GFP-mRNA n = 3; VEGF-C-mRNA, n = 5). Experiment was repeated independently with similar results. **e** Mice were inoculated with 50,000 GL261-Luc cells and treated with Luc-mRNA or VEGF-C-mRNA at day 7. Tumor inoculated brain hemisphere was collected and analyzed using FACS (n = 3; 3 animals were pooled for each n). **e** Number of CD3-positive cells (n = 3; 3 animals were pooled for each n). Data are mean ± S.D. *P < 0.05; **P < 0.01; ***P <0.001; ****P<0.0001 (two-tailed unpaired Student's t-test, two-sided Log-rank Mantel-Cox test).

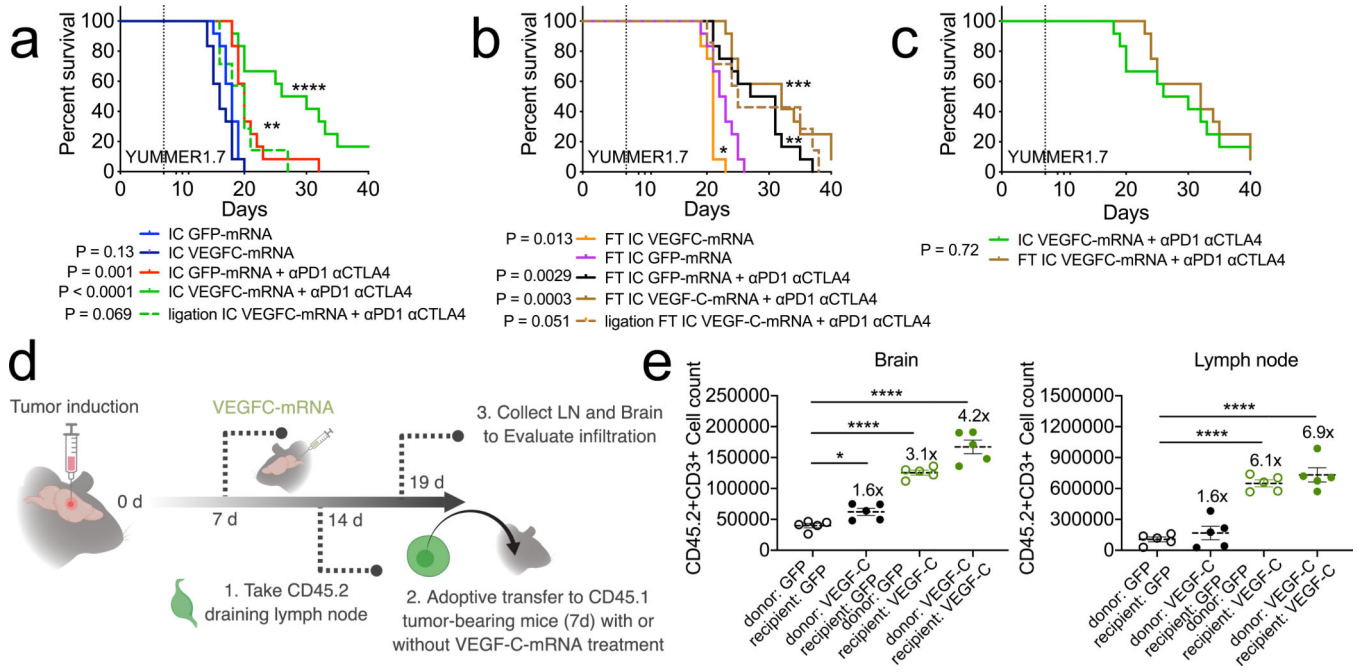

Figure 4. T cell extrinsic VEGF-C signaling mediates protection against intracranial tumor and is equivalent to peripheral priming.

a-c mice were given either only YUMMER1.7 intracranial tumors (IC, **a**) or a YUMMER1.7 flank tumor and YUMMER1.7 intracranial tumor (FT, **b**) and treated with GFP/VEGF-C-mRNA on day 7 and anti-PD1 (RMP1–14), anti-CTLA4 (9H10) on days 7, 9 and 11. (**a,** n = 12 for all groups except ligation IC VEGFC-mRNA + αPD1 αCTLA4, n = 7; **b**, n = 12 for all groups except ligation FT IC VEGFC-mRNA + αPD1 αCTLA4, n = 7). **d** Schematic for experiment design of **e**. Congenic CD45.2 mice were injected with GL261 tumors. 7 days post tumor inoculation (pti), mice were treated with GFP-mRNA or VEGF-C-mRNA. At 7 days post mRNA-treatment (14 day-pti) leukocytes from dcLNs were transferred into congenic CD45.1 mice bearing 7 day-tumors. Five days after transfer, dcLNs and brain tissues were harvested to analyze T cell infiltration. **e** Quantification of brain infiltrating and lymph node T cells (n = 5 animals, all groups). Data are mean ± S.E.M *P < 0.05; **P < 0.01; ***P <0.001; ****P<0.0001 (two-tailed unpaired Student's t-test, two-sided Log-rank Mantel-Cox test)